NEUTRON INDUCED ALPHA PRODUCTION FROM CARBON BETWEEN 18 AND 22 MeV

A.P. STEVENS

A thesis submitted to the
University of Cape Town
in partial fulfillment of the
conditions for the degree of
Master of Science

October 1976

ABSTRACT

Cross sections for neutron induced alpha production in carbon were measured at seventeen energies between 18 and 22 MeV, using a deuterated anthracene crystal as both target and detector. Pulse shape discrimination was employed to separate the alphas and elastically scattered deuterons from the other reaction products. Published (n,d) elastic scattering data were used as a standard to obtain the alpha production cross sections. Comparison with available measurements shows good agreement.

ACKNOWLEDGEMENTS

The author wishes to thank the following:

His supervisor, Prof. F.D. Brooks, for his assistance, encouragement and support;

The South African Atomic Energy Board for financial assistance and the use of their facilities;

The staff of the Southern Universities Nuclear Institute for their co-operation;

Drs. D.W. Mingay and J. White for their comments and criticisms, and for proof reading this manuscript;

His parents for their interest and encouragement;

His wife for her fortitude, support and encouragement, and for typing this manuscript.

INDEX

LIST OF FIGURES

LIST OF TABLES

CHAPTER 1

INTRODUCTION

1.1 Background

A need exists for carbon cross section data in a number of fields (La75). Nuclear data are, for instance, needed by the medical profession where neutron beams are to be used for radiotherapy. Alpha producing reactions are major contributors to the total cross section above 12 MeV (La75), where the two dominant reactions yielding alpha particles are $^{12}C(n,\alpha)^{9}Be$ and $^{12}C(n,n')3\alpha$. The various possible mechanisms for these reactions are shown in Figure 1.1, overlaid on a diagrammatic representation of the energy levels of the participating nuclei.

There is essentially only one mechanism yielding a single alpha particle and that is the $^{12}C(n,\alpha_0)^{9}Be$ reaction - Path I(a) in Figure 1.1. This reaction, with a threshold at 6,181 MeV, leaves the ^{9}Be in its ground state. The $^{12}C(n,\alpha_i)^{9}Be^{*}$ reaction leading to excited states of ^{9}Be contributes essentially only to the $^{12}C(n,n')3\alpha$ reaction (La75) as these levels are unbound to decays via both the $^{12}C(n,\alpha_i)^{9}Be^{*}(n')^{8}Be^{*}(2\alpha)$ and the $^{12}C(n,\alpha_i)^{9}Be^{*}(\alpha)^{5}He^{*}(n')\alpha$ reactions - Paths I(b) and I(c) in Figure 1.1.

Decay of excited states of ^{12}C can also produce three alphas, the threshold being at 7,887 MeV neutron energy. These excited states are populated by either inelastic scattering on ^{12}C or neutron emission from the compound nucleus, ^{13}C, and can either form three alphas directly by three-body breakup (Path II(a)) or can decay sequentially via alpha emission to ^{8}Be, which is unbound to further alpha emission (Path II(b)). The final possibility for producing three alphas is the four-body breakup of ^{13}C into a neutron and three alphas (Path III). The

3/possibilities

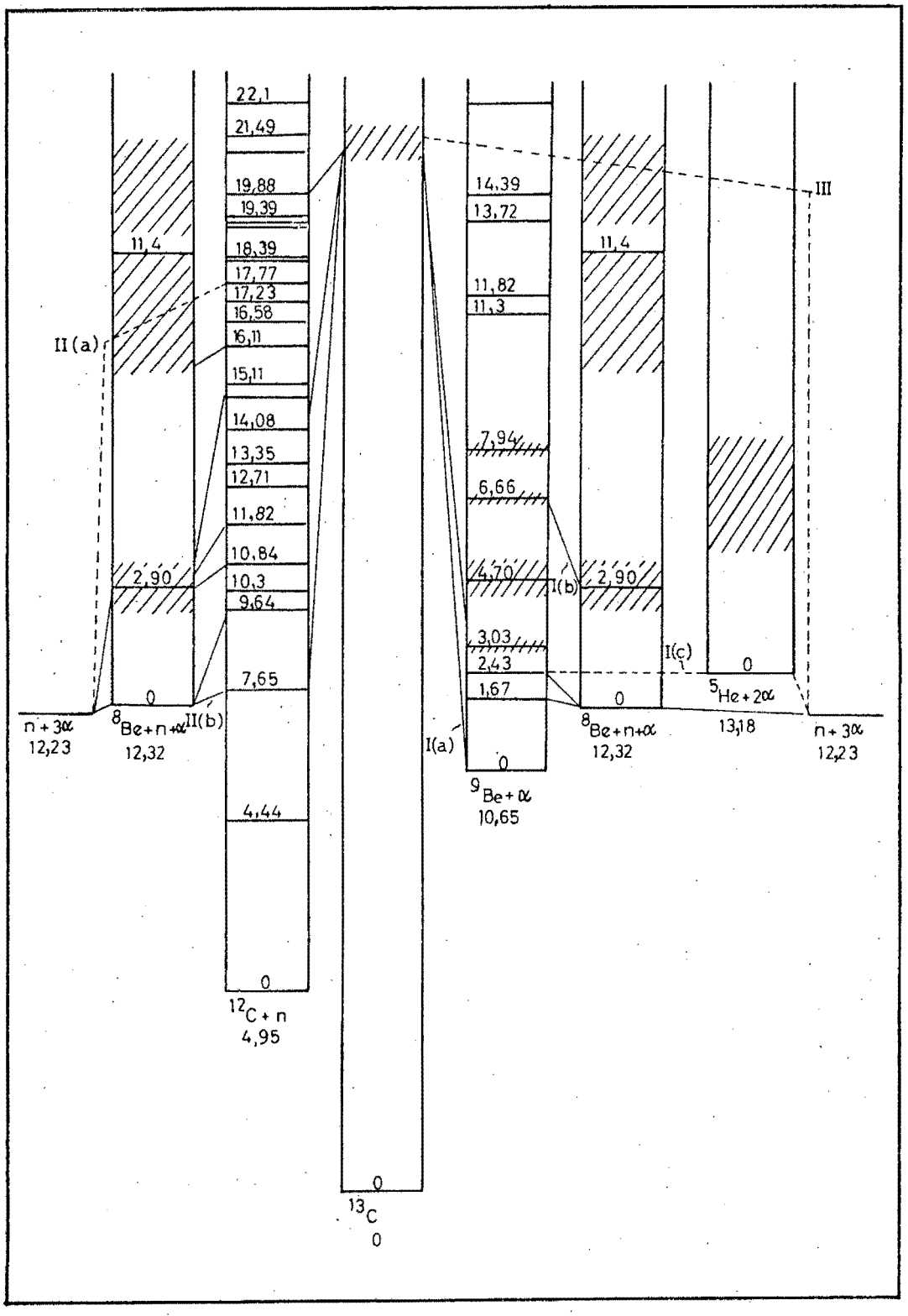

Figure 1.1

Diagrammatic representation of the energy levels of the participating nuclei showing possible reaction paths. All energies shown are in units of MeV.

possibilities open as mechanisms of the $^{12}C(n,n')3\alpha$ reaction are therefore:

(i) $^{12}C(n,\alpha)^{9}Be^{*}(n')^{8}Be^{*}(2\alpha)$
(ii) $^{12}C(n,\alpha)^{9}Be^{*}(\alpha)^{5}He^{*}(n',\alpha)$
(iii) $^{12}C(n,n')^{12}C^{*}(\alpha)^{8}Be^{*}(2\alpha)$
(iv) $^{12}C(n,n')^{12}C^{*}(3\alpha)$
(v) $^{12}C(n,n',3\alpha)$ - four-body breakup.

A number of experiments have been performed to investigate the mechanisms operating in this reaction (Gr49, Pe51, Ja53, Fr55, and Br64) and are reviewed in a report by Lachkar et al (La75). The studies conclude that the reaction proceeds via some sequential process with no evidence for simultaneous breakup for neutron energies up to 20 MeV. Lachkar et al (La75) deduce that approximately 80% of the $^{12}C(n,n')3\alpha$ cross section comes from inelastic scattering, leaving the ^{12}C in some state above 7,653 MeV. The remaining 20% is attributed to the $^{12}C(n,\alpha)^{9}Be$ reaction, with the ^{9}Be nucleus in the 2,43 MeV state decaying via 2α + n emission.

Shackleton (Sh70) investigated the $^{12}C(n,n')3\alpha$ reaction at a neutron energy of 22 MeV using pulse shape discrimination techniques. Subsequently a far more sophisticated data handling facility has been installed at the Southern Universities Nuclear Institute, and it was decided to extend this measurement to cover a range of neutron energies. This extension was especially interesting since preliminary studies showed the possibility of strong energy dependence of the cross section in the excitation function, which is not only of instrinsic importance, but also of potential interest for practical applications like, for example, radiotherapy.

Lachkar et al (La75) have produced evaluated cross sections for the two reactions from their thresholds up

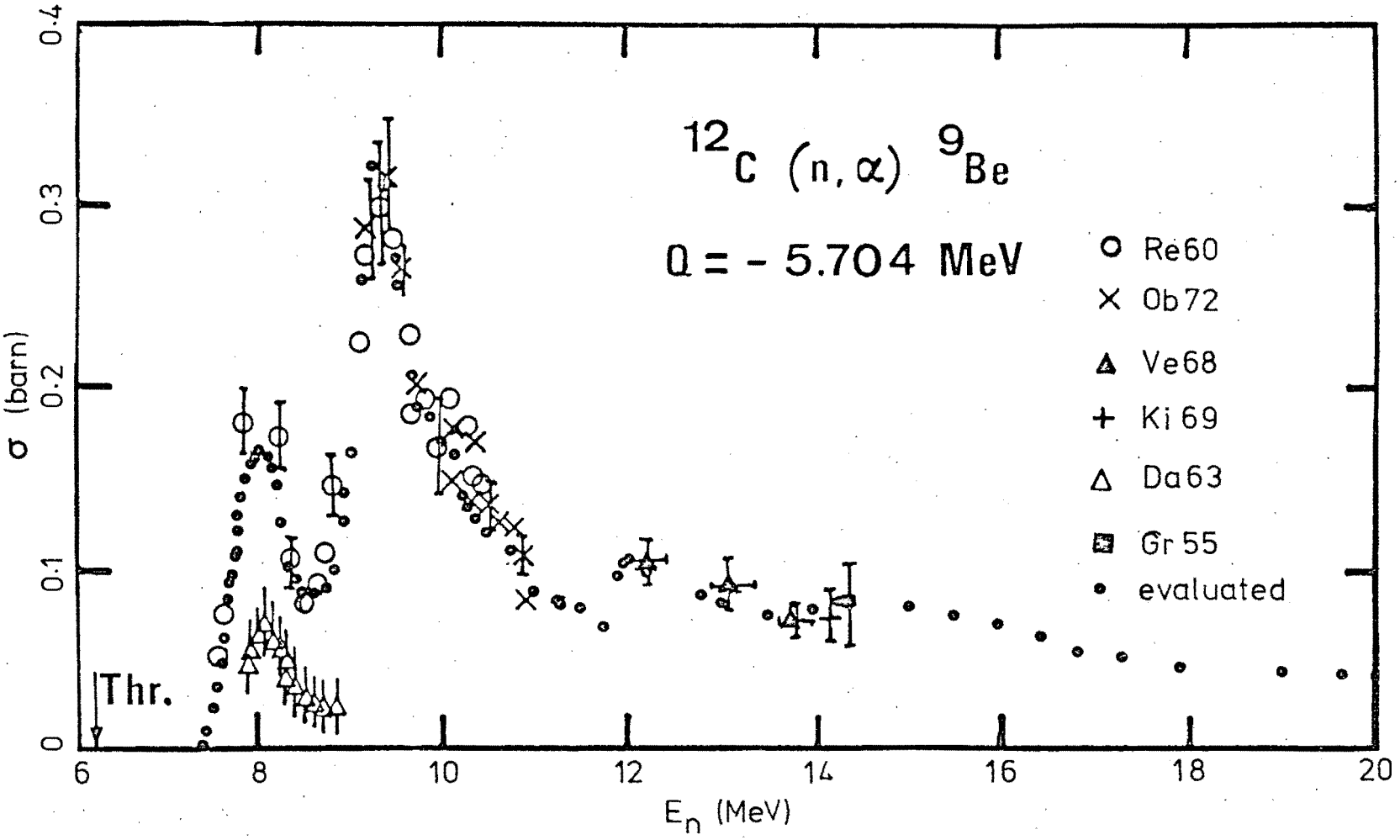

Figure 1.2

Compilation of cross section data for the $^{12}C(n,\alpha)^{9}Be$ ground state reaction. References for the points are presented in the figure. This is a reproduction from the report by Lachkar et al (La75).

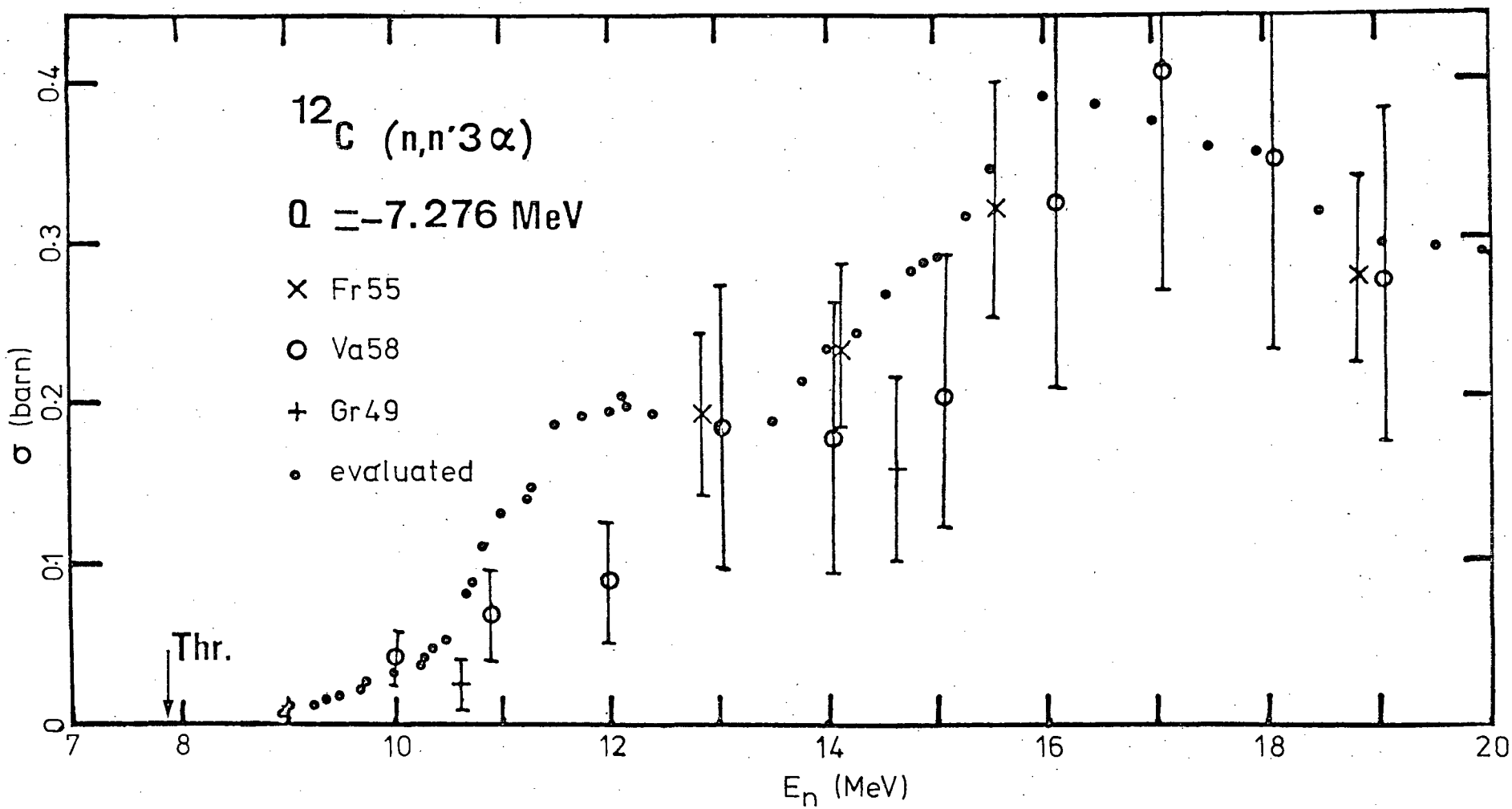

Figure 1.3

Compilation of available data for the $^{12}C(n,n')3\alpha$ reaction. References for the results presented are shown in the figure. This diagram is a reproduction from the report by Lachkar et al (La75).

to 20 MeV neutron energy. Their data are presented in Figures 1.2 and 1.3. There is a need for data in the $^{12}C(n,\alpha)^{9}Be$ reaction above 14,1 MeV, and for the $^{12}C(n,n')3\alpha$ reaction above 19 MeV.

1.2 The Experiment

The experiment was conducted using a method similar to that employed by Pauletta (Pa73/5) in an (n,d) breakup experiment. This consisted of obtaining energy spectra for alphas and elastically scattered deuterons at a number of neutron energies. The integrals of these spectra were then compared in order to calculate the cross sections for alpha production, using the accurate (n,d) elastic scattering data.

A deuterated organic scintillator was used both as neutron target and as detector. It was coupled to a photomultiplier fitted with a pulse shape discrimination (PSD) circuit, to separate deuteron and alpha produced scintillations. Because both alpha and recoil deuteron spectra were needed for analysis, it was necessary to have a very wide dynamic range with good resolution at low energies. This was accomplished by tuning the PSD circuit to an optimum setting, and by processing the incoming data with a data acquisition programme, developed to incorporate facilities for examining spectra in fine detail.

In summary, the experiment was conducted using organic scintillators and PSD techniques to produce alpha and deuteron spectra. These were then analysed to yield alpha production cross sections.

7 /1.3 Expected

1.3 Expected Alpha Pulse Height Spectrum

A consideration of the expected alpha pulse height (L) spectrum, for an experiment of this type, is useful at this stage as it will clarify some of the later discussion. The L spectrum is composed of contributions from the $^{12}C(n,\alpha)^{9}Be$ and the $^{12}C(n,n')3\alpha$ reactions. The shapes of these component spectra are determined by the non-linear response of the crystal (Br56) and the fact that any scintillation processed is the sum of the scintillations produced by each charged reaction product detected. These two factors ensure that the response due to three alphas each of energy E is less than the response due to one alpha of energy 3E. The summation process also causes any structure in the $^{12}C(n,n')3\alpha$ spectrum, due to decays of specific levels of ^{12}C, to be 'smeared' out as the initial alpha, which has an energy characteristic of this decay, cannot be detected separately from the other two, which have a random distribution of energy. The summation process together with the non-linear response also cause a partial separation of the contributions due to the two competing reactions.

The energy available to each reaction is approximately the same, but in the $^{12}C(n,n')3\alpha$ reaction this energy is shared by three alphas and a neutron, which is not detected; while in the $^{12}C(n,\alpha)^{9}Be$ reaction it is divided between an alpha and a ^{9}Be nucleus, both of which are detected. The removal of energy by the undetected neutron, together with the non-linear response and the summation process ensure that the maximum response for the $^{12}C(n,\alpha)^{9}Be$ reaction is greater than for the $^{12}C(n,n')3\alpha$ reaction. This implies that the upper end of the alpha spectrum can be expected to be due to the $^{12}C(n,\alpha)^{9}Be$ reaction only. Its contribution to the total alpha yield can then be determined by fitting an analytic spectrum for this reaction to the high L tail

of the alpha spectrum. The remainder after subtracting this contribution, can then be assumed to be due to the $^{12}C(n,n')3\alpha$ reaction. It will be shown later, in Chapter 4, how analytically generated spectra for the two reactions are used to separate their contributions from the experimental spectra.

1.4 Summary of Objectives

Shackleton's work (Sh70) demonstrated the feasibility of using organic scintillators and PSD techniques for investigating alpha producing reactions of carbon. Pauletta (Pa73/5) has shown how the elastically scattered deuteron spectra obtained by utilising a deuterated organic scintillator can be used to provide accurate calibration in cross section measurements of this type. This experiment was conducted primarily to measure total alpha production cross sections for carbon, irrespective of the method of production, by making use of a deuterated anthracene crystal and pulse shape discrimination. Cross sections were measured at a number of neutron energies to investigate the possibility of strong energy dependence in the excitation function. The final objective was to determine individual cross sections for the $^{12}C(n,\alpha)^{9}Be$ and $^{12}C(n,n')3\alpha$ reactions.

CHAPTER 2

EXPERIMENTAL SET-UP

2.1 Neutron Production

Neutrons were obtained from the $T(d,n)^4He$ reaction, using a gaseous tritium target and a deuteron beam from the 6 MV Van der Graaff accelerator of the Southern Universities Nuclear Institute. The target was held in a cylindrical cell of diameter 1 cm and length 3 cm, placed with its long axis along the beam direction. The gas was kept at a nominal pressure of ~0,5 atmospheres.

Two convenient methods may be employed to vary the energy of the neutrons incident on the detector. The first makes use of the kinematics of the reaction and involves moving the detector so that neutrons emerging at different angles, θ, relative to the beam are detected. This can be seen by referring to Figure 2.1, for deuterons of 5,0 MeV entering the tritium cell. The second method involves keeping θ constant while varying the energy of the incident deuterons. The first method is simpler, as any change made to the deuteron energy requires readjustment of the accelerator.

If θ is ~90°, a significant energy spread is found in the neutrons entering the detector, because of the finite solid angle presented, involving both an angular acceptance $\Delta\theta = \theta' - \theta''$ (Figure 2.2(a)) and the maximum value of $dE_n/d\theta$. This spread is shown in Figure 2.3. To avoid this uncertainty in the energy it was decided to limit θ to less than 20°, where the energy spread is defined predominantly by beam energy loss in the target, and to vary the deuteron energy.

A pulsed beam was used because time of flight measurements

13/were

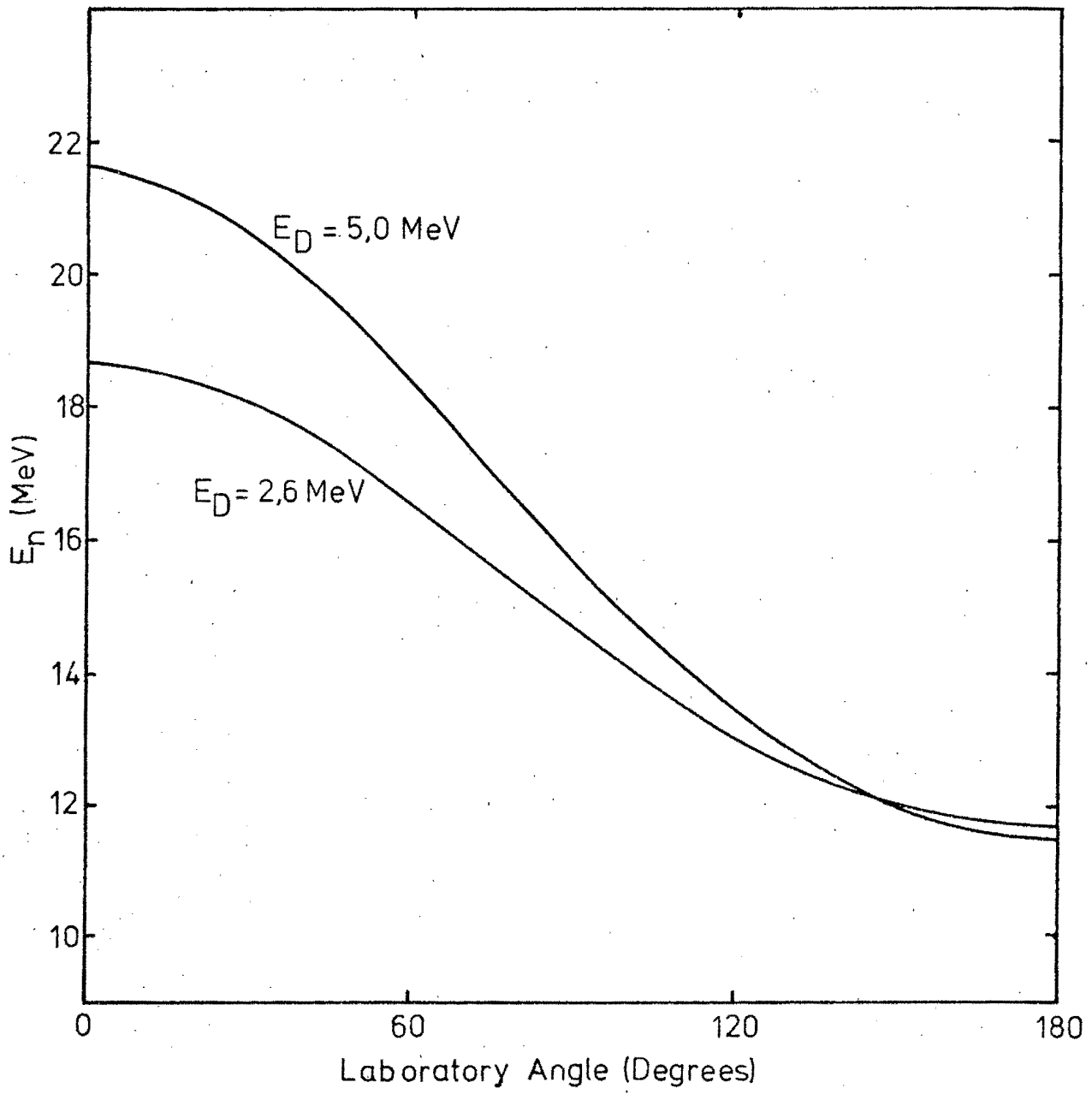

Figure 2.1

Graphic representation of the dependence of neutron energy on angle of emission in the laboratory frame, for the $T(d,n)^4He$ reaction at 5,0 and 2,6 MeV deuteron energies. These were the maximum and minimum deuteron energies obtainable during this experiment.

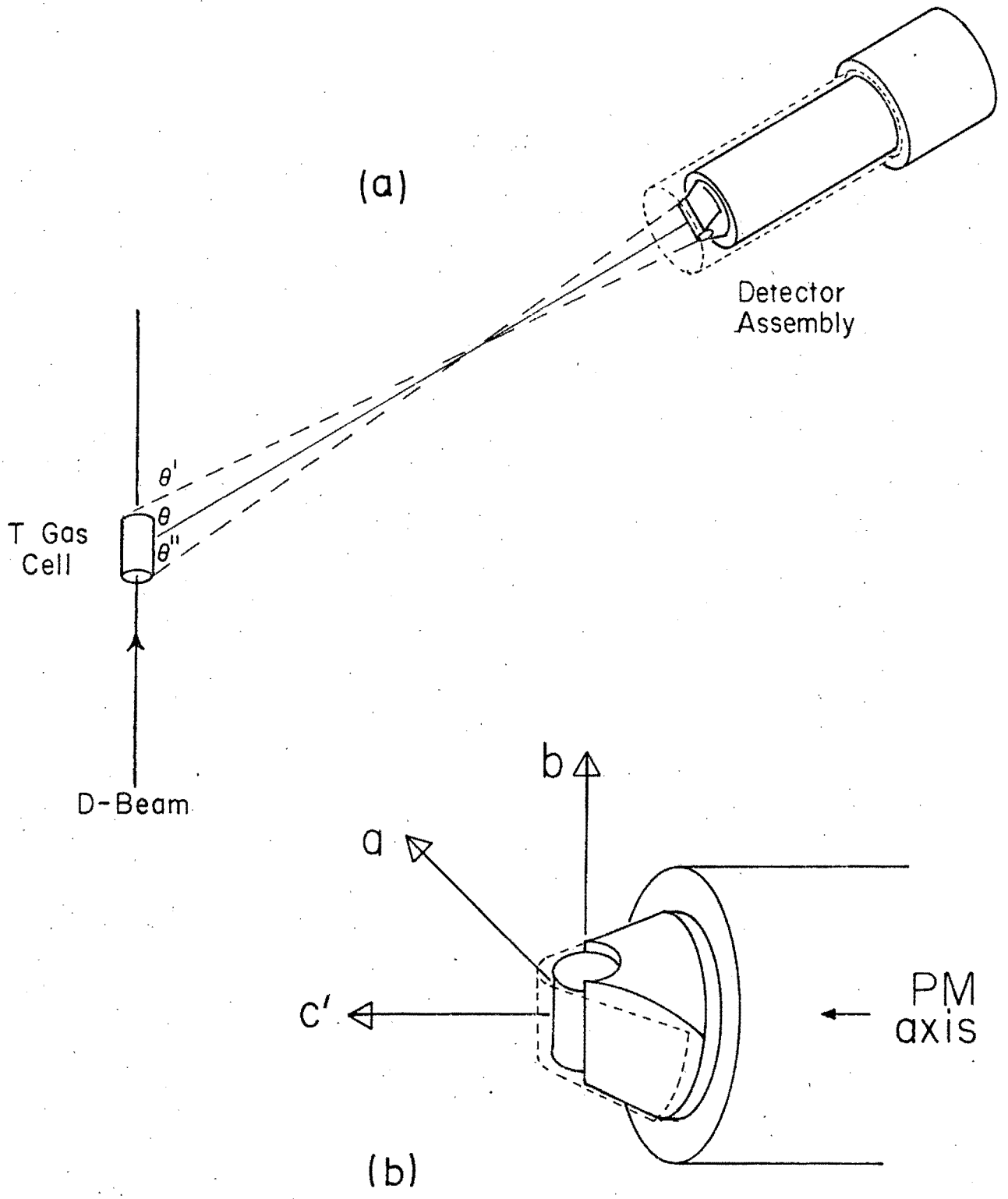

Figure 2.2

(a) Experimental configuration showing the positioning of the detector relative to the tritium gas cell. θ' and θ'' represent the limiting angles of emission for neutrons detected by the detector.

(b) Crystal mounted on photomultiplier in its light pipe assembly. The arrows labelled a, b and c' indicate the orientation of the crystal axes, and the dotted lines show the position of the reflector used to

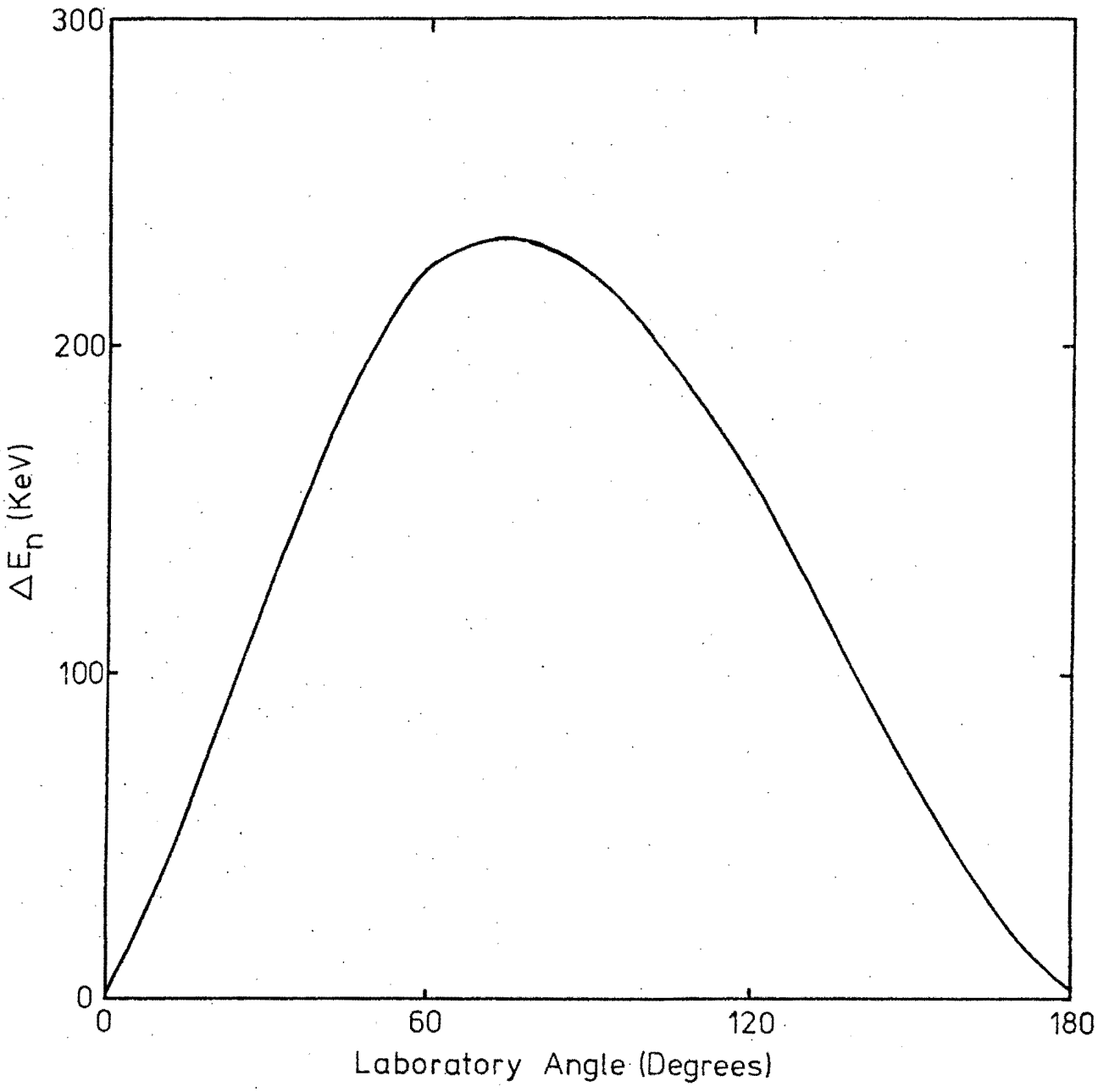

Figure 2.3

Graphic representation of neutron energy spread as a function of angle θ - see Figure 2.2(a). The case presented here is for 5,0 MeV deuterons entering the tritium gas cell, and a flight path of 60 cm.

were needed to ensure that only mono-energetic neutrons were considered. Figure 2.4 shows a time of flight spectrum obtained for a flight path of 60 cm, with a neutron peak, a gamma peak, and background. The data acquisition system allowed a "window" to be set on the neutron peak, thus selecting the primary neutrons from the $T(d,n)^4He$ reaction.

2.2 Detection of Reaction Products

The use of a deuterated anthracene crystal as target and detector allowed alpha and calibration deuteron spectra to be collected simultaneously. The crystal was a cylinder of diameter 1 cm and length 2,1 cm, with the b axis of the crystal parallel to the cylinder axis. It was mounted on the photomultiplier using the light pipe and reflector assembly shown in Figure 2.2(a). The crystal exhibits pulse height anisotropy depending on the direction of motion of the detected particle relative to the crystal axes (Br74). The crystal was orientated to align the c' axis with the incident neutron beam, since this orientation gave maximum resolution by PSD.

The photomultiplier was fitted with a PSD circuit (Pa73) which produced a pulse, S, characteristic of the scintillation decay, and, therefore, of the ionising particle producing it. The energy of the particle was deduced from the integrated scintillation output, L. These signals, together with a timing pulse from the beam pick-off, were fed through the circuit shown in block form in Figure 2.5 to the on-line computer. This analysed L and S in coincidence to produce a 64 x 64 two parameter spectrum as shown in Figure 2.6. In this analysis each type of ionising radiation produces a unique locus or 'ridge' in the LS plane, so enabling separation of the different reaction products.

18/2.3 Data

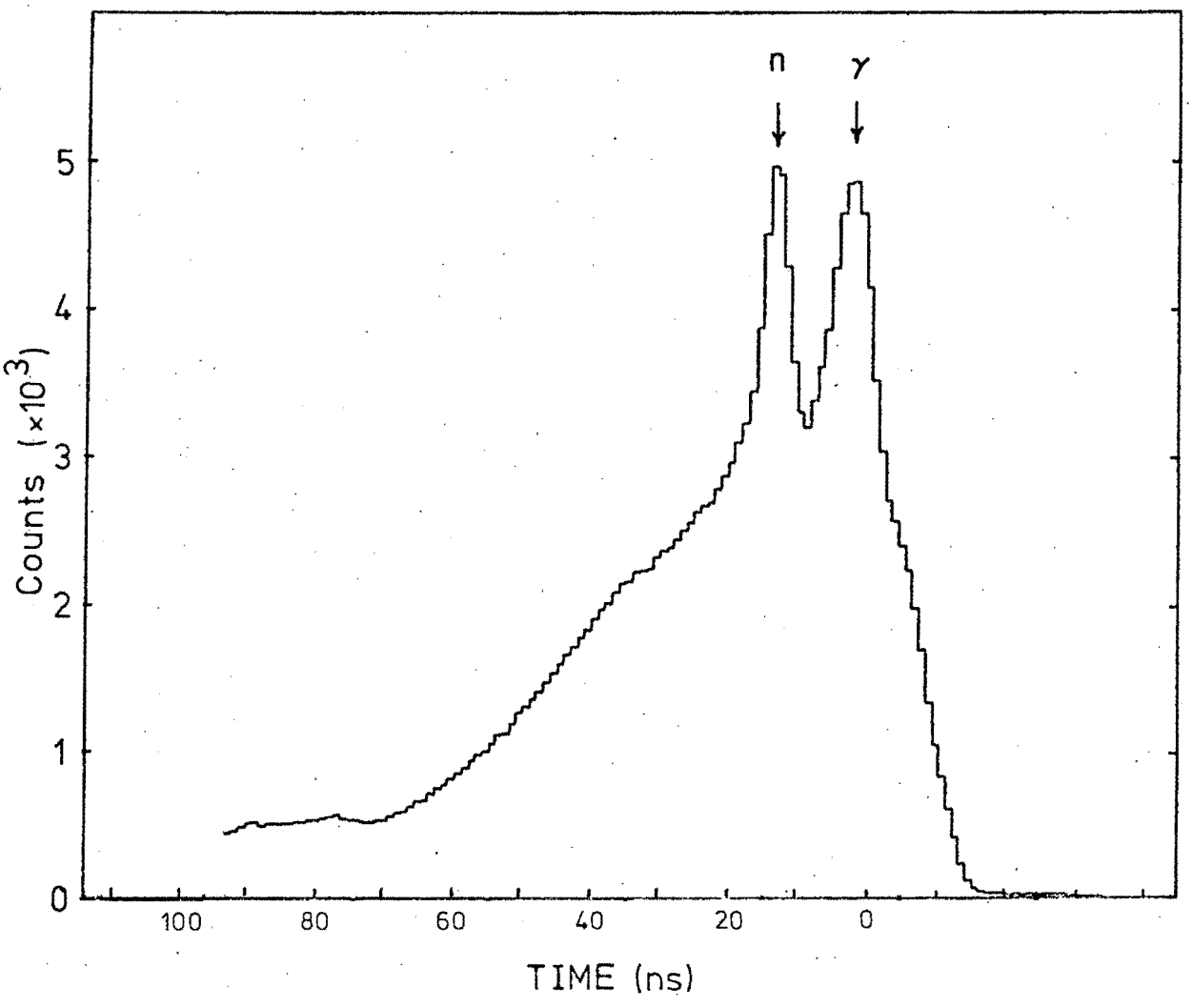

Figure 2.4

A typical time of flight spectrum. The twin peaks, labelled n and γ, are due to primary neutrons from the $T(d,n)^4He$ reaction and to target gamma rays respectively.

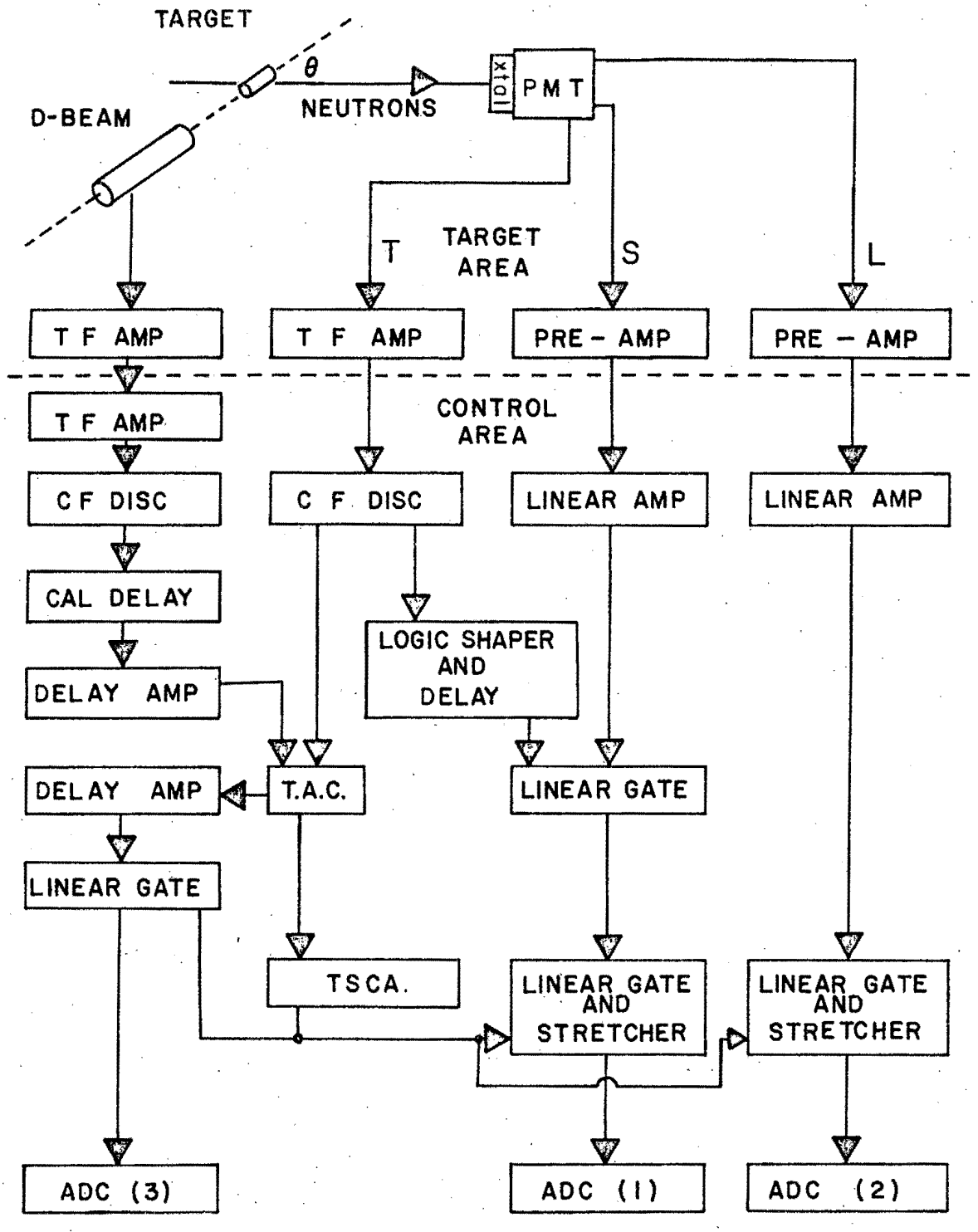

Figure 2.5

The electronic circuit used for this experiment, shown in block form. The three analogue to digital converters (ADC's) were interfaced to the on-line PDP-15 computer.

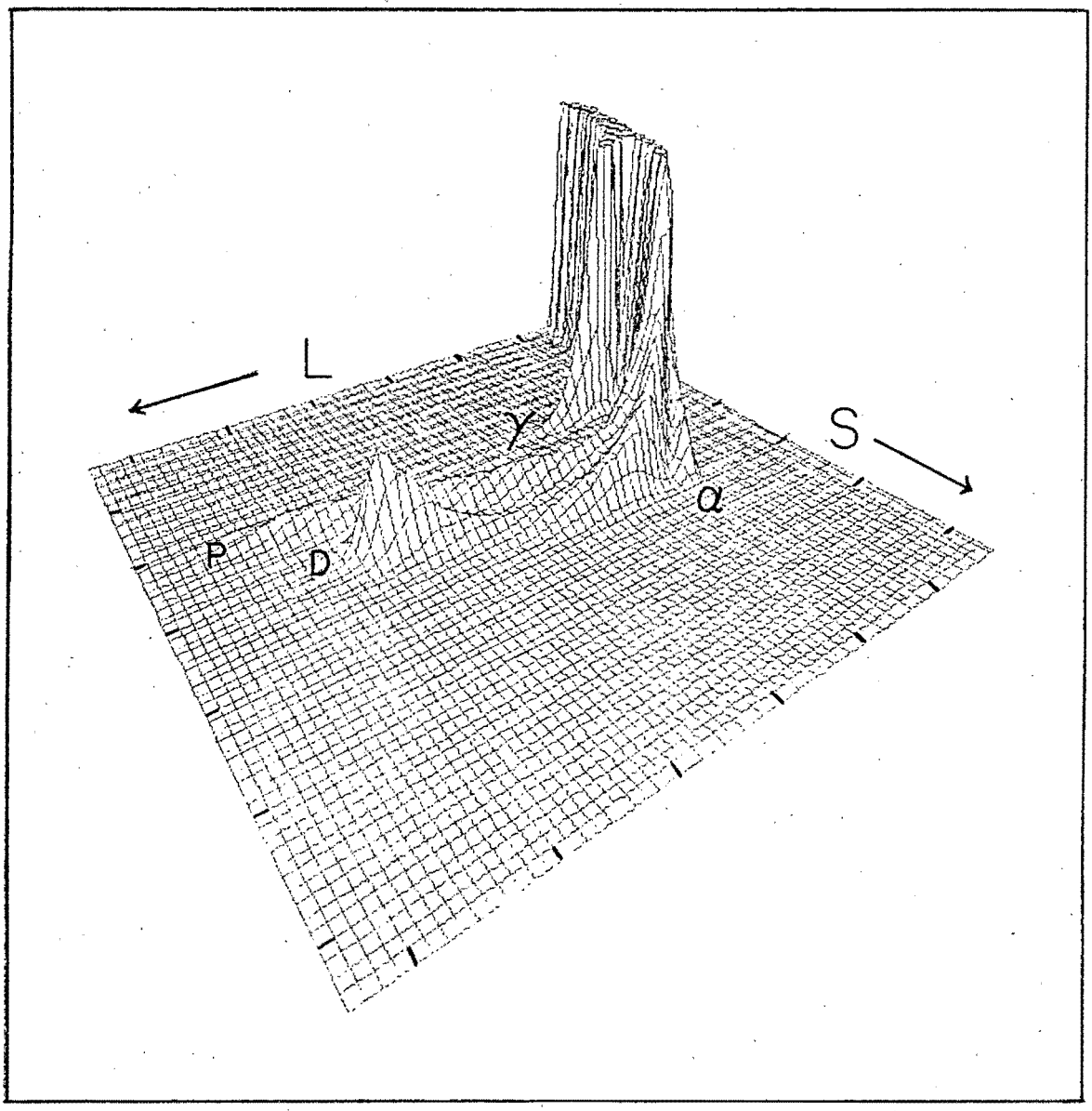

FULL LS SPECTRUM

Figure 2.6(a)

Isometric representation of a full LS spectrum obtained for 20 MeV neutrons incident on the deuterated anthracene crystal. The 'ridges' labelled α, γ, P and D are due to detected alpha particles, gamma rays, protons and deuterons respectively.

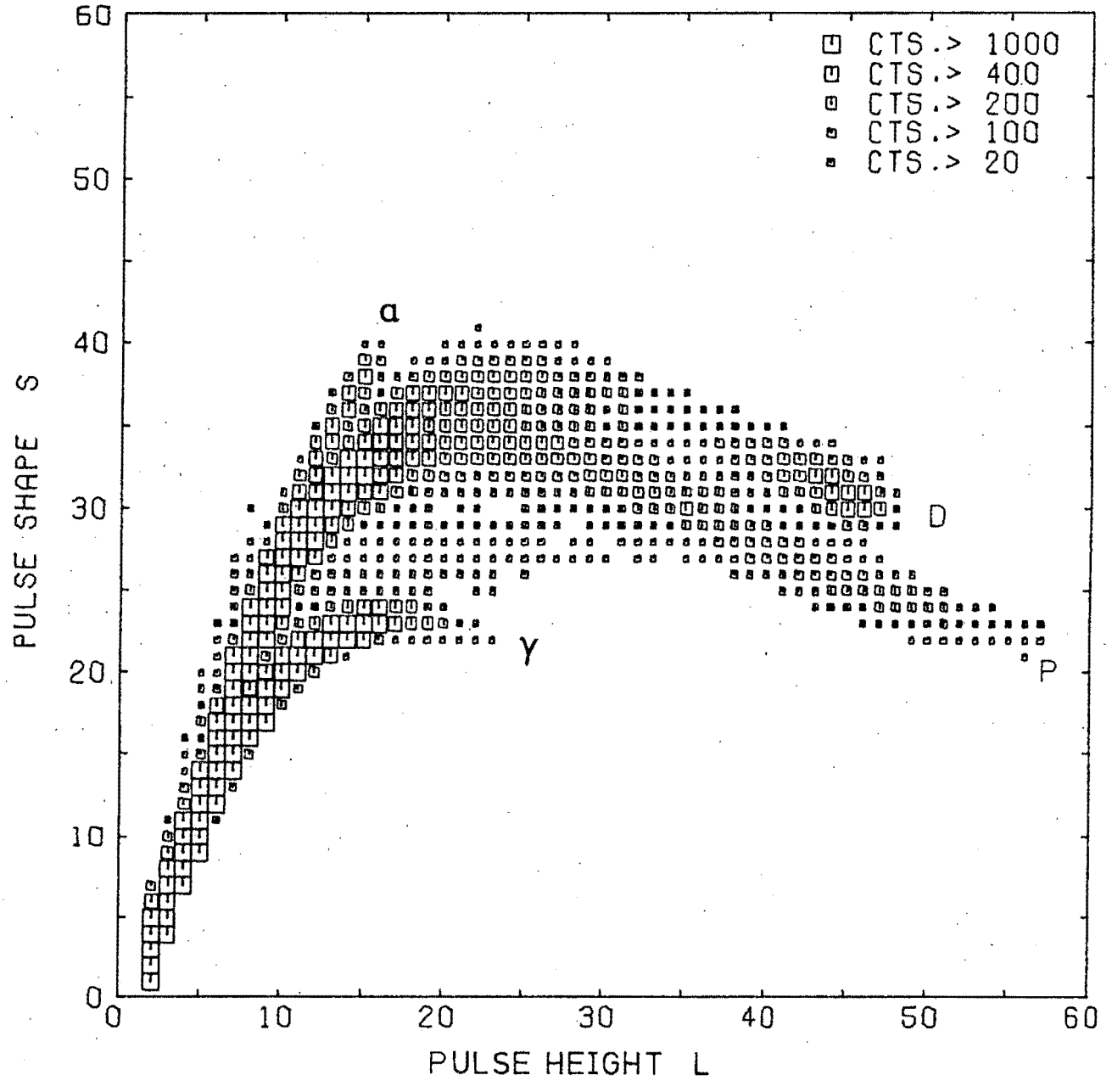

Figure 2.6(b)

Density plot of the LS spectrum shown in Figure 2.6(a). The labelling is consistent with that used in Figure 2.6(a).

2.3 Data Acquisition System

A new data acquisition programme was developed for this experiment, to enhance the resolution of the alpha particles at low energies and to satisfy the need for detailed monitoring of incoming data. The programme was written to accept "events" characterised by three parameters (L, S and T in this case), each digitised to binary words between eight and twelve bits in length.

The aim was then to use one parameter (T) as a select/reject parameter and to form a two parameter (LS) spectrum for events so selected in a 4096 element array, usually in a 64 x 64 configuration. For this 64 x 64 configuration the programme selects six bits of L and six bits of S. These selected bits can be any group of six contiguous bits of the eight to twelve collected. The most significant bits are, however, normally chosen. During data acquisition, 256 channel spectra are formed for three selected regions of the LS spectrum and also for the select/reject parameter (T).

The collected data are stored on magnetic tape as acquired, i.e. all the bits are saved. This tape can be scanned off-line with offsets and shifts on any parameter, so that selected regions of interest in the LS spectrum can be viewed in more detail (Figure 2.7).

A system of displays was also provided, to allow continuous and detailed monitoring of all phases of data acquisition. The programme proved very useful in the collection of experimental data and the preparation thereof for final analysis on the UNIVAC 1106 at the University of Cape Town, and is discussed in more detail in Appendix A.

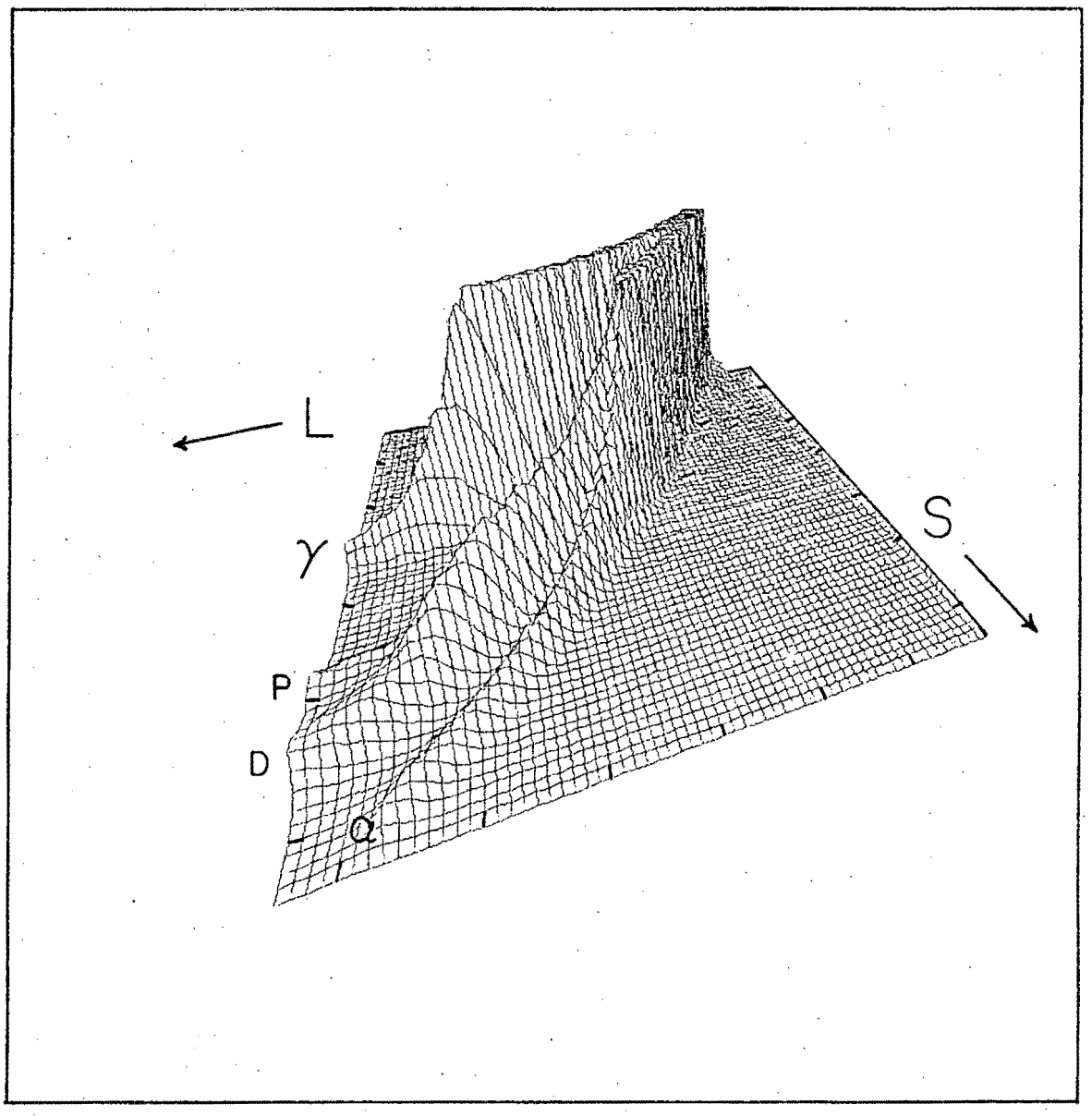

EXPANDED LS SPECTRUM

Figure 2.7(a)

Isometric representation of the expanded LS spectrum produced by reprocessing the data stored on magnetic tape during the formation of the LS spectrum shown in Figure 2.6. (Incident neutron energy was 20 MeV.) The ridges labelled α, Y, P and D were produced by alphas, gammas, protons and deuterons respectively. The convergence of the alpha and proton/deuteron 'ridges' is obtained in more detail, thus facilitating more accurate separation at lower energies.

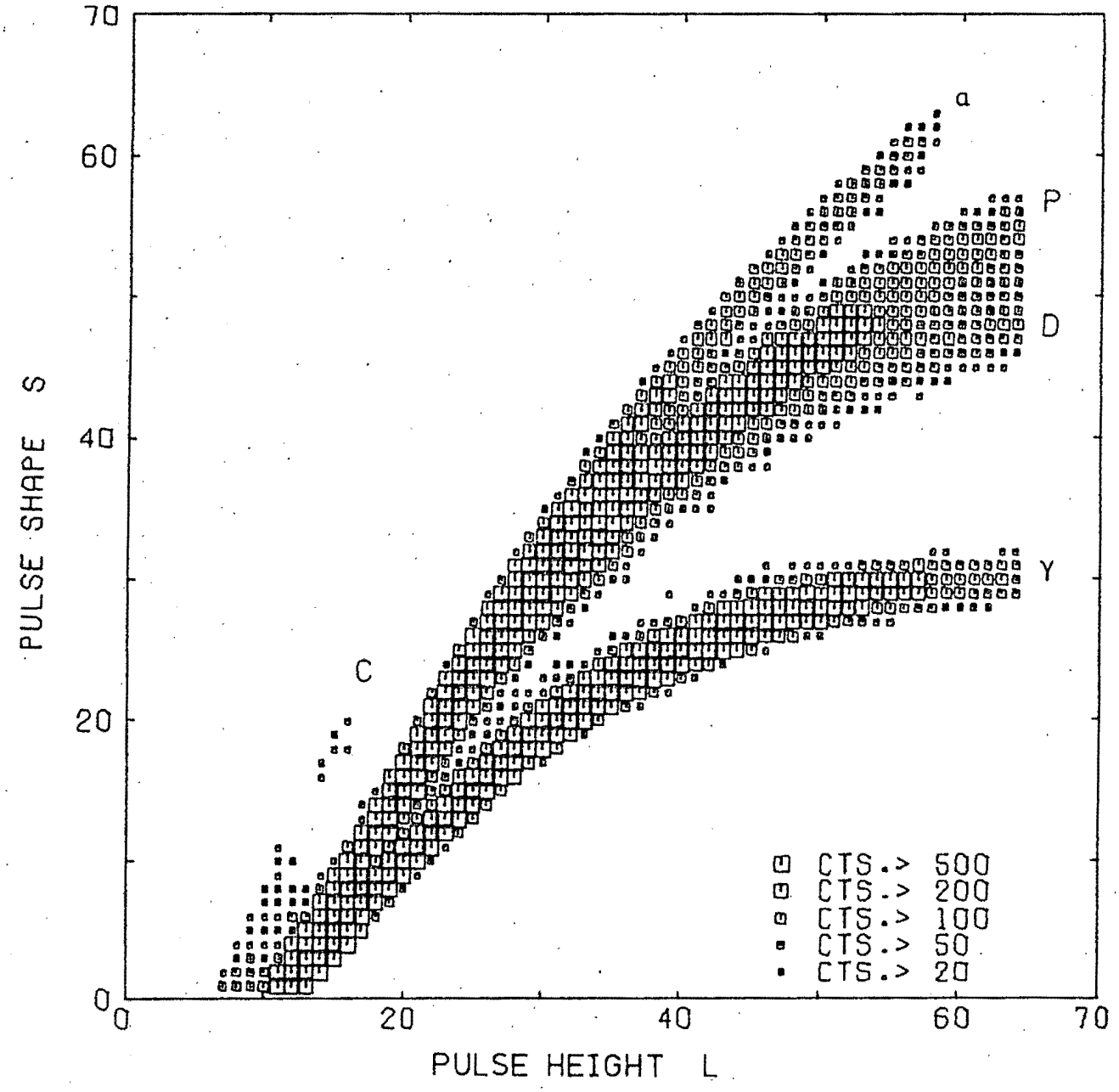

Figure 2.7(b)

Density plot of the LS spectrum shown in Figure 2.7(a). The additional locus, C, is believed to be due to recoil carbon atoms from elastic scattering. It is not readily visible in Figure 2.7(a) because of the method of presentation.

CHAPTER 3

THE EXPERIMENT

3.1 Preparations

Prior to running any experiments, the angular dependence of the energy of the neutrons emitted by the $T(d,n)^4He$ reaction was calculated, using the formula shown in Figure 3.1 obtained from Marion and Young (Ma68). The incident deuteron energy was corrected for losses sustained in passing through the Havar window of the gas cell, and through the tritium itself. The losses in the Havar window were calculated for a composition as given in Marion and Young (Ma68) and a thickness of 0,00352 gcm^{-2}. Tritium gas losses were evaluated at a temperature of 15°C and a pressure of 760 mm Hg. The losses obtained are presented in Figure 3.2, while an energy versus angle curve is shown in Figure 2.1.

The energy spread in the neutrons due to the geometry of the experimental set-up was also calculated as a function of angle. Figure 2.8 shows this spread as a function of angle at an incident deuteron energy of 5,0 MeV. The ΔE shown is the maximum deviation from the neutron energy expected at the angle given. These two sets of curves were needed for determining which angles and deuteron energies to use so that neutron energies could be duplicated with different geometries, while still keeping the dispersion to a minimum.

3.2 Experimental Procedure

The experiment was set up as shown in Figure 2.2, using a flight path of 60 cm between the gas cell and the detector. Runs at different angles (θ) and deuteron

24/energy

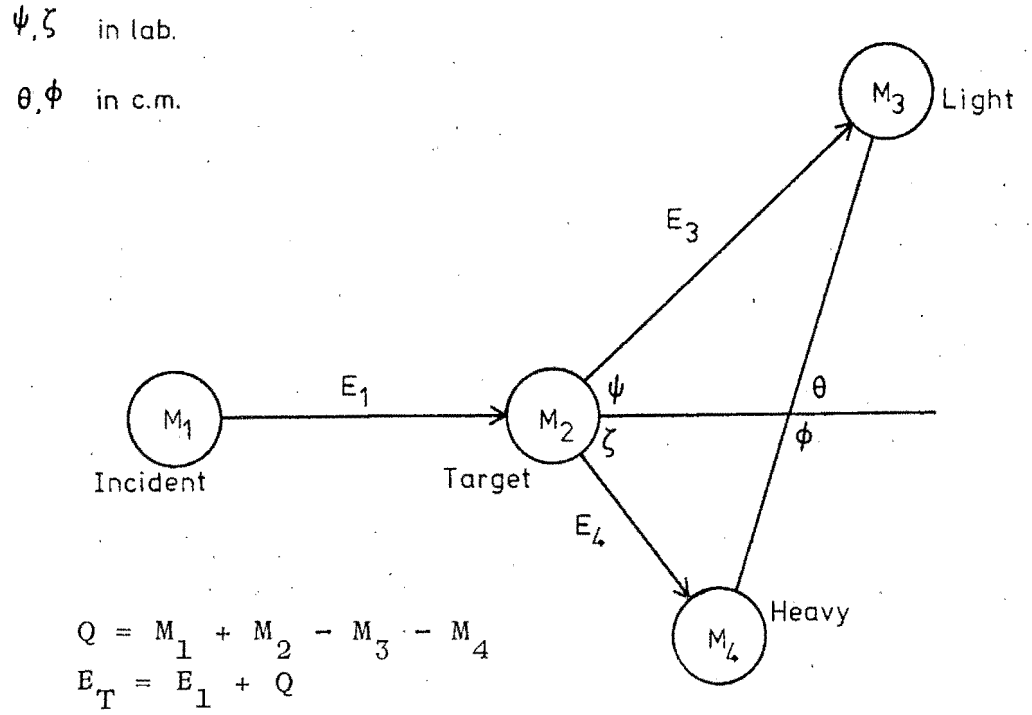

$$Q = M_1 + M_2 - M_3 - M_4$$
$$E_T = E_1 + Q$$

Define:

$$A = \frac{M_1 M_4 (E_1/E_T)}{(M_1 + M_2)(M_3 + M_4)}$$

$$B = \frac{M_1 M_3 (E_1/E_T)}{(M_1 + M_2)(M_3 + M_4)}$$

$$C = \frac{M_2 M_3}{(M_1 + M_2)(M_3 + M_4)}\left[1 + \frac{M_1 Q}{M_2 E_T}\right]$$

$$D = \frac{M_2 M_4}{(M_1 + M_2)(M_3 + M_4)}\left[1 + \frac{M_1 Q}{M_2 E_T}\right]$$

The laboratory energy of the light product is then given by the equation:

$$\frac{E_3}{E_T} = B + D + 2(AC)^{\frac{1}{2}}\cos\theta$$
$$= B\left[\cos\psi + (D/B - \sin^2\psi)^{\frac{1}{2}}\right]^2$$

Figure 3.1

Formula used for calculating the neutron energy from the $T(d,n)^4He$ reaction and also for the Monte Carlo model of the $^{12}C(n,\alpha)^9Be$ reaction. (Reproduced from Marion and Young (Ma68).)

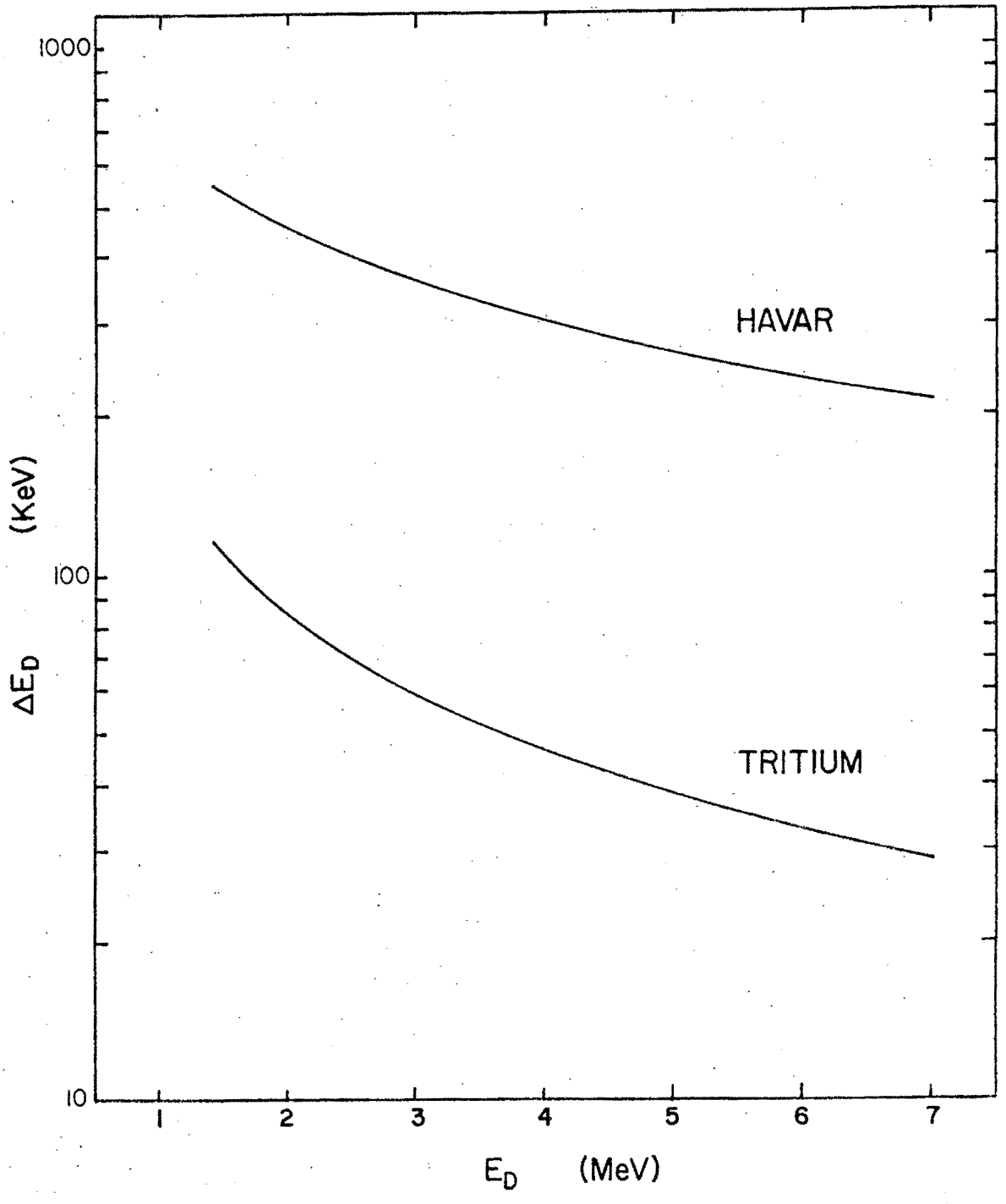

Figure 3.2

Energy losses for deuterons passing into the tritium gas cell. The losses due to the Havar foil window on the gas cell were calculated for a composition as quoted by Marion and Young (Ma68) and a thickness of 0,00352 g cm^{-2}. Losses in the tritium were calculated for a temperature of 15°C and a pressure of 760 mm Hg (Ma75).

energy settings were selected to cover as wide a neutron energy range as possible, while, at the same time, keeping the energy spread to a minimum. The neutron energies considered during this experiment are shown in Table 3.1. The lower limit on the energies was imposed by the decision to limit θ to less than 20°, as it was found impossible to produce a pulsed deuteron beam below 2,6 MeV with sufficient current to activate the beam-line timing pick-off. The allowable terminal voltage defined the upper limit.

Preliminary time of flight and LS spectra were produced at each energy setting. The former were needed for setting the selected timing "window", while the latter allowed boundaries to be set, dividing the LS spectrum into three regions. These in turn allowed rough LS spectra to be produced for the protons, deuterons and alphas during the main run. These L spectra were useful in monitoring the incoming data. These preliminary LS spectra also allowed a check to be made for any electronic drifts.

It was also found necessary to check the analogue to digital converters at intervals during the experiment. This was especially necessary since the zero offsets could drift, and in so doing, upset the L axis calibration of the LS spectrum. The check was carried out by observing the relative positions of the Compton edges produced by a ^{60}Co source at normal and double gain.

The incoming data were monitored at all stages of collection to detect and avoid electronic drifts or other malfunctions. All accepted events were buffered on magnetic tape to be used later for analysis of expanded views of selected regions of the LS spectrum. On completion of a run the accumulated LS spectrum and its associated projected spectra were written onto a second magnetic tape. The buffered data were then processed to

26/generate

E_D (MeV)	θ (degrees)	E_N (MeV)	ΔE_N (MeV)
4,8	0	21,46	0,28
4,6	0	21,22	0,29
4,4	0	20,98	0,30
4,2	0	20,73	0,31
4,0	0	20,48	0,32
3,8	0	20,23	0,33
4,0	20	20,14	0,38
3,6	0	19,98	0,34
3,8	20	19,90	0,39
3,4	0	19,72	0,36
3,2	0	19,46	0,37
3,0	0	19,20	0,38
3,0	10	19,12	0,41
2,8	0	18,93	0,39
3,0	20	18,91	0,46
2,6	0	18,65	0,41

Table 3.1

The neutron energies considered for this experiment are shown together with the angles and deuteron energies at which they were obtained. The spread in the neutron energy was determined by considering both the deuteron energy loss in the gas cell and the spread due to the finite geometry of the gas cell and the anthracene crystal.

generate an expanded LS spectrum showing the region where the alpha and deuteron ridges merged, as shown in Figures 2.7. This was necessary as accurate stripping of the alpha and deuteron spectra was needed, to as low an energy as possible. These sets of LS spectra were processed as explained in the next chapter, to yield the alpha production cross sections.

CHAPTER 4

DATA ANALYSIS

4.1 Separation of Alpha and Deuteron Spectra

The analysis required the separation of the alpha and deuteron contributions from the experimental LS spectra. This was done using a programme available on the UNIVAC 1106 (Pa73/5). The stripping is accomplished by considering the S spectra at each L value of the LS spectra individually. The single particle contributions to these S spectra are assumed to be Gaussian in form. A re-iterative, linear least squares method is employed to fit these Gaussian curves to the data, optimising their positions, widths and heights to achieve the best fit between their sum and the experimental data. Figure 4.1 shows the fitting carried out on the LS spectrum of Figure 2.7 for L values between 26 and 30. Constraints and checks are provided to ensure good fits wherever possible, and to reject the stripped values if a good fit could not be achieved.

The full LS spectra were processed to yield deuteron L spectra while alpha L spectra were obtained from the expanded LS spectra. Examples of L spectra obtained in this manner are shown in Figure 4.2. The spectra shown are the deuteron and alpha contributions to the LS spectra shown in Figure 2.6 and 2.7 respectively. The cut-off represents the lowest L at which the alpha and deuteron loci could be reliably resolved.

4.2 Analysis of Alpha Spectra

In order to separate the $^{12}C(n,\alpha)^{9}Be$ and $^{12}C(n,n')3\alpha$ contributions from the stripped alpha spectra, it was decided that analytic spectra produced by Monte Carlo

30/models

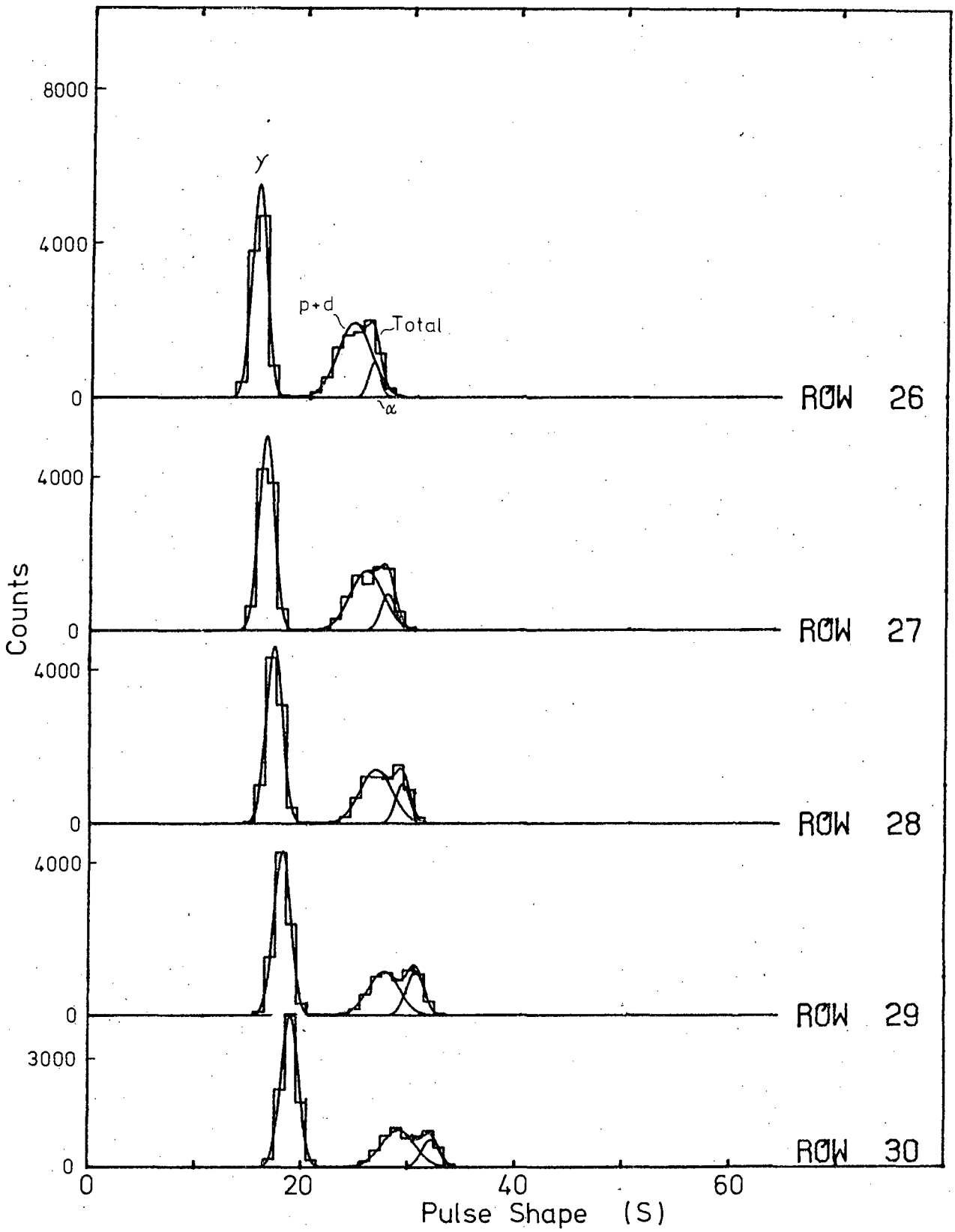

Figure 4.1

Stripping of the alpha contribution from the LS spectrum shown in Figure 2.7, for L values between 26 and 30. The histograms represent the experimental data, while the fitted Gaussians and their sum are shown by smooth curves.

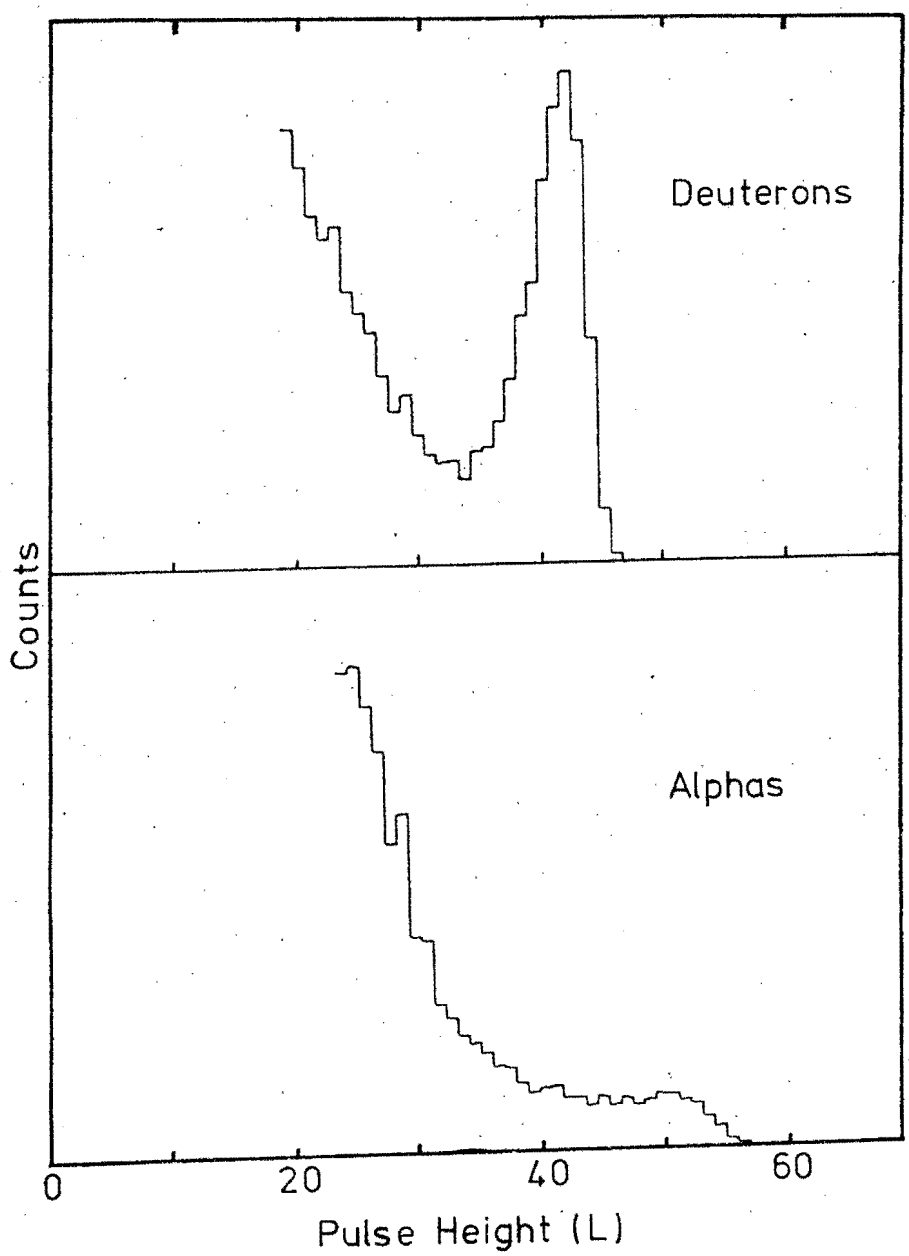

Figure 4.2

Deuteron and alpha L spectra produced by stripping their contributions from the normal and expanded LS spectra shown in Figures 2.6 and 2.7 respectively. The 'counts' axes are linear in both cases and the scales have been chosen to show the structure to greatest advantage.

models would be fitted to the data. (The models are described below and flowcharts of the programmes are presented in Appendix B.) It was, therefore, necessary to calibrate the response of the detector to the energy of the detected particles. The deuteron spectra were used for this calibration as the high L cut-off of the recoil deuteron 'bump' is sharp (see Figure 4.2) and corresponds to a kinematically well defined energy. Furthermore it was necessary to take the true position of zero L into consideration - as discussed in Section 3.2. The calibration was carried out using Brooks' response curves for anthracene (Br56) and Pauletta's relation for deuteron response (Pa73/5), viz.

$$L_D(E) = 2L_p(\tfrac{1}{2}E)$$

The $^{12}C(n,\alpha)^{9}Be$ reaction was modelled using the formula presented in Figure 3.1. Isotropic emission of the alphas in the centre of mass frame was assumed, with the angle of emission being generated randomly. The effects of the recoiling ^{9}Be nucleus were also included. The light output of the detector is the sum of the responses to the alpha particle and the ^{9}Be nucleus. The ^{9}Be will, therefore, tend to compensate for the energy spread of the alphas as it has maximum energy when the alpha has minimum and vice versa. In order to calculate the response of the crystal to the ^{9}Be a charge state of 2+ was assumed at all energies. This approximation caused a slightly more pronounced compensation than would be expected as the response was too high for high energy ^{9}Be nuclei and too low for those with low energy. The effect is small, however, as the light output is due mainly to the alpha particles. It was also necessary to include the Coulomb barrier penetrability of the alphas (Fe53). An example of an L spectrum generated by this model is shown in Figure 4.3, while the corresponding energy spectrum is shown in Figure 4.4.

33/The

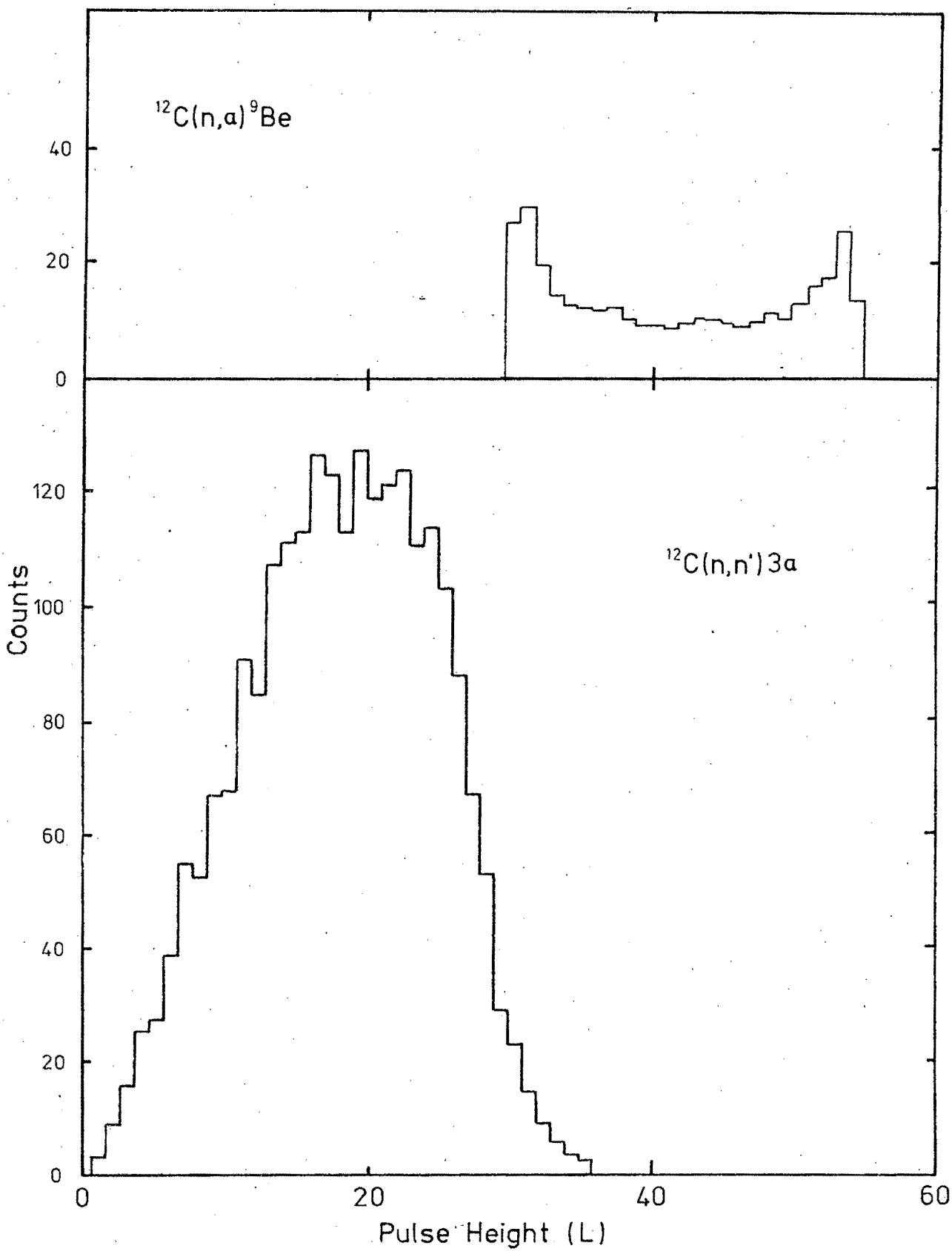

Figure 4.3

L spectra produced by the Monte Carlo models of the two competing reactions, at a neutron energy of 20 MeV. The integrals have been normalised to the cross sections of Lachkar et al (La75).

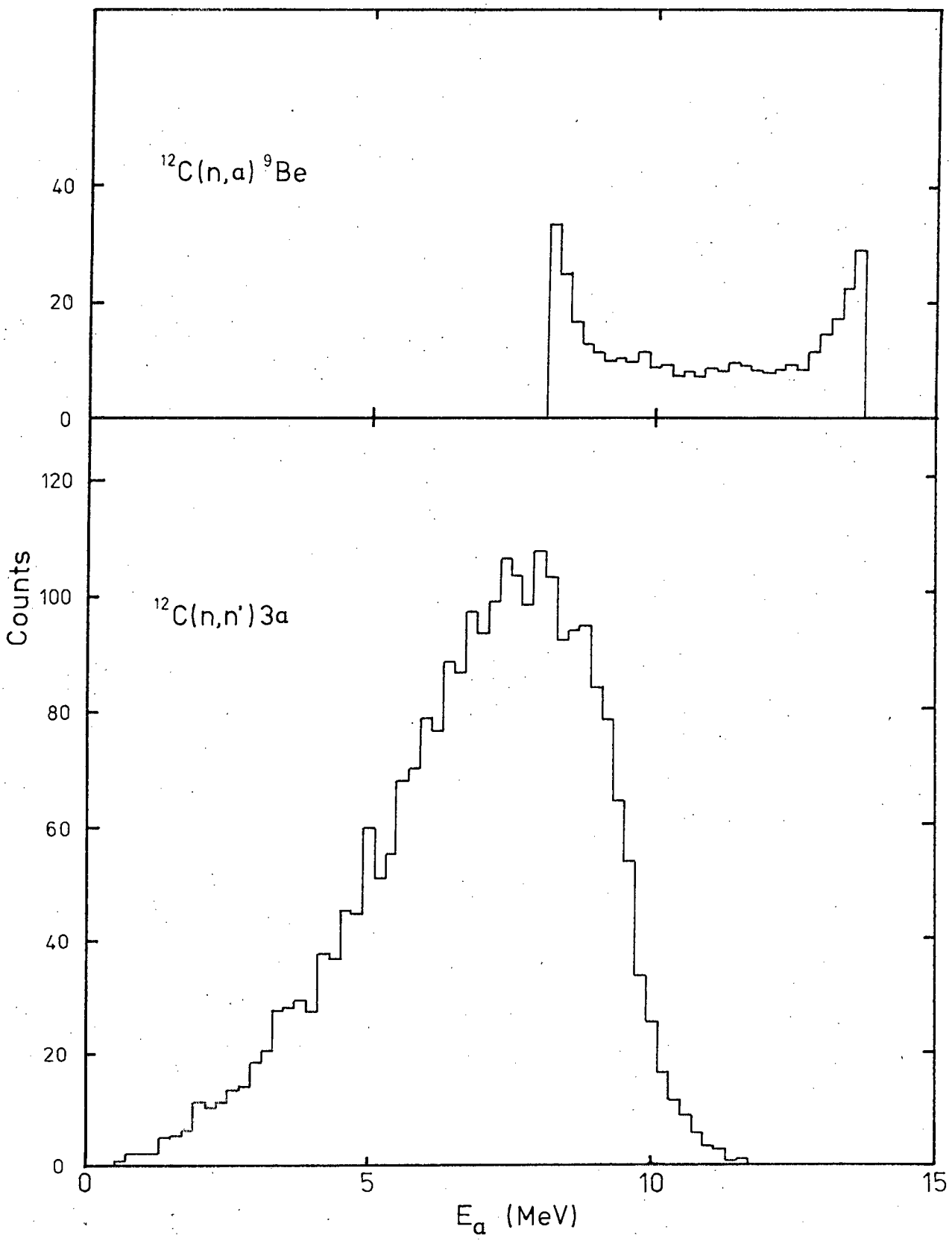

Figure 4.4

Energy spectra produced by the Monte Carlo models of the two competing reactions, at a neutron energy of 20 MeV. The integrals have been normalised to the cross sections of Lachkar et al (La75).

The $^{12}C(n,n')3\alpha$ reaction was analysed using a four particle phase space energy distribution for the reaction products. This is again an approximation as it is generally accepted that the reaction proceeds via some sequential process (La75). Frye et al (Fr55), however, find good agreement between the phase space distribution and their data. They explain this by observing that the sequential process proceeds mainly via the 2,90 MeV state in ^{8}Be (see Figure 1.1). The width of this state, together with the fact that the last two alphas would be expected to follow some sort of statistical distribution in the centre of mass frame, could produce an energy distribution similar to that predicted by phase space considerations. The other reason for choosing this simplified approach is that a model of the sequential process is complicated and time consuming on the computer, a fairly simple model taking approximately twenty times as long as the phase space model. The phase space distribution used was that employed by Frye et al (Fr55), namely:

$$N(\varepsilon)d\varepsilon = A\sqrt{\varepsilon}\,(1-\varepsilon)^{2}d\varepsilon$$

where A is a constant and ε is the ratio of the energy of the alpha particle to the maximum energy it can have. This distribution was sampled randomly, while implementing the response summation process to produce the L and energy spectra for this reaction, examples of which are shown in Figures 4.3 and 4.4 respectively.

Before matching the analytic and experimental spectra it was necessary to take the finite resolution of the detector into account. The 'smeared' L spectrum obtained by considering this finite resolution is given by (Pa73):

$$I'(L) = \int_{0}^{Lmax} I(L')R(L-L')dL'$$

where I(L) is the L distribution, and R(L-L') the resolution

34/function

function, which can be approximated by the Gaussian distribution:

$$R(L-L') = \frac{1}{2\sqrt{\pi\sigma}} \exp\left[-(L-L')^2/2\sigma^2\right]$$

for cases involving a large number of photons and Poisson statistics (Bi64). Birks (Bi64) also shows that, to a good approximation

$$\sigma^2 = SL$$

where S is a constant. Furthermore, the response function was introduced by means of a table of values obtained from Brooks' response curves (Br56). The spectra in Figure 4.5 show the effect of this convolution on the spectra in Figure 4.3. The convolution causes a smearing of the spectra. The $^{12}C(n,n')3\alpha$ spectrum also exhibited a major change of form. This was caused by the L dependence of σ ($\sigma^2 = SL$) and the fact that the spectrum was non-zero at low L values. The Gaussian resolution function was much narrower at low L than at high L. This caused the narrowing of the peak, the shifting of the peak position towards higher L, and the flatter slope on the low L side of the peak.

In order to obtain the best fit to the data it was necessary to determine σ. This was done by matching the upper end of the convoluted $^{12}C(n,\alpha)^9Be$ spectrum to the upper end of the experimental spectrum. This had to be approached in a devious manner as σ only determines the amount of 'smearing', while the fitting must take the relative magnitudes of the two spectra into account as well. For this reason a Gaussian curve was fitted to the upper end of the experimental spectrum being considered. Its standard deviation is an indication of the smearing and is independent of its maximum value. In fitting the convoluted analytic spectra to the data to obtain σ, a

36 /similar

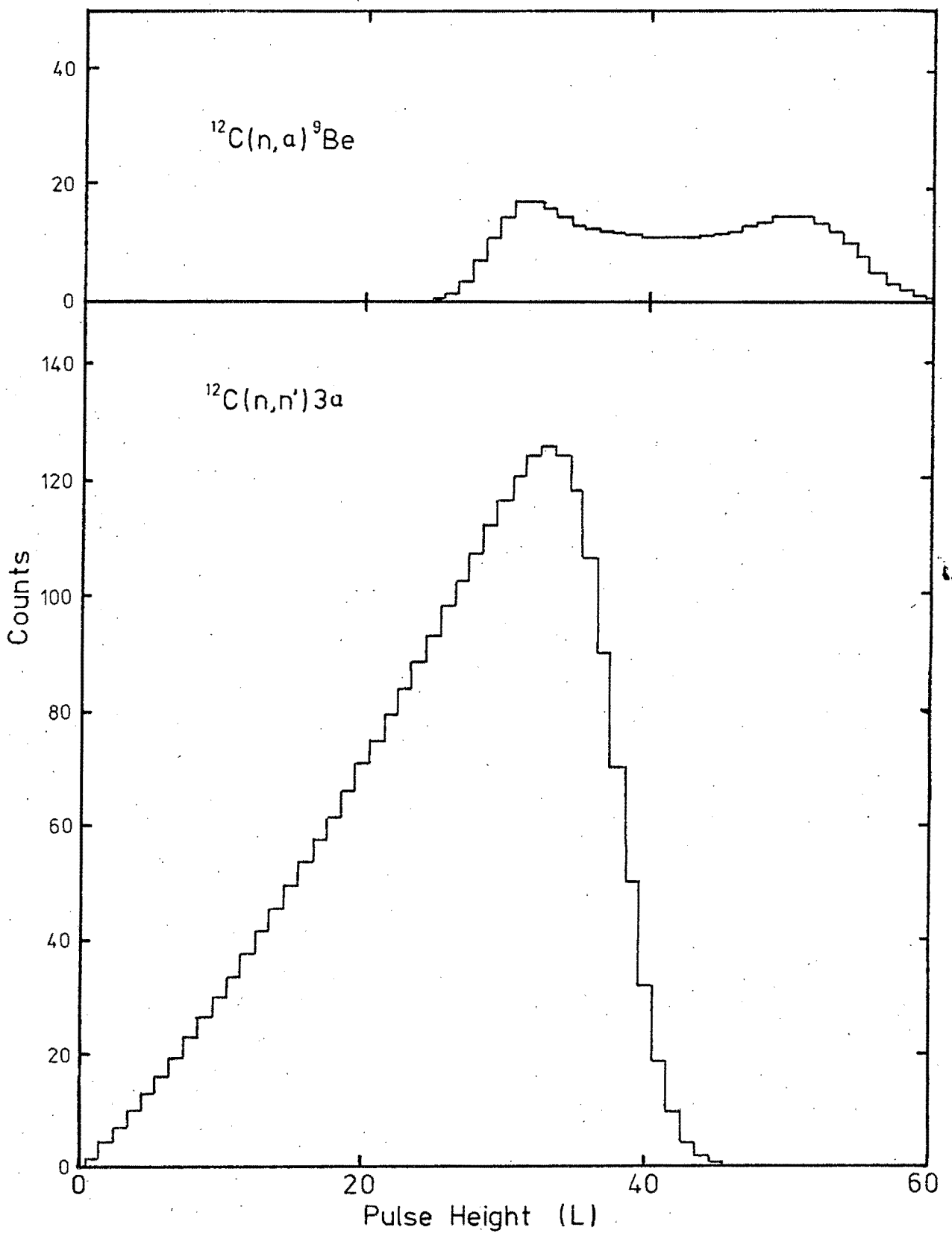

Figure 4.5

L spectra produced by convoluting those shown in Figure 4.3 with a Gaussian resolution function. The integrals are normalised to the cross sections of Lachkar et al (La75).

similar procedure was followed. At each approximation of σ a Gaussian curve was fitted to the upper end of the analytic spectrum, and σ adjusted to match the standard deviations of the Gaussians fitted to the analytic and experimental spectra. The heights of the two Gaussians obtained, provided a means for normalising the analytic spectrum. This normalised, convoluted analytic spectrum was assumed to be the $^{12}C(n,\alpha)^{9}Be$ contribtuion and was subtracted from the experimental spectrum. It remained to convolute the $^{12}C(n,n')3\alpha$ analytic spectrum, taking the σ obtained as described above and to fit it to the residual experimental data by normalisation. The integrals of the analytic spectra after fitting were then used to calculate the cross sections, as is discussed in the next chapter.

CHAPTER 5

RESULTS AND CONCLUSIONS

5.1 Calculation of Cross Sections

Cross sections for alpha production via the two processes available were calculated using a method similar to that used by Pauletta (Pa73/5) to determine (n,d) breakup cross sections. This involves using the available (n,d) elastic scattering data as a standard and leads to the reaction:

$$\sigma_a = \frac{10}{14} \frac{I_a}{I_D} \sigma_D$$

where: I_a is the integral of the relevant component of the alpha spectrum;

I_D is the integral of the deuteron spectrum;

σ_D is the total cross section for (n,d) elastic scattering; and

$\frac{10}{14}$ is a constant required as the chemical structure of deuterated anthracene is $C_{14}D_{10}$.

It is not possible, however, to carry out the calculation in this manner as the full deuteron spectrum cannot be stripped from the LS spectrum. The forward recoil deuteron 'bump' is used instead, as it can be accurately stripped and integrated. Pauletta (Pa73) calculated the cross sections, $\sigma_{D'}$, for this forward recoil 'bump' at a number of energies, from the available elastic scattering data, and his values were used. The alpha production cross section is, therefore, calculated as follows:

$$\sigma_a = \frac{10}{14} \frac{I_a}{I_{D'}} \sigma_{D'}$$

where $I_{D'}$ is the integral of the forward recoil 'bump'. The cross sections obtained are shown in Figures 5.1, 5.2

42/and

E_n (MeV)	$\sigma_{n,a}$ (mb)	σ_{3a} (mb)	σ_{TOTAL} (mb)
21,46 ± 0,28	31,0 ± 10,9	143 ± 50	174 ± 61
21,22 ± 0,29	23,3 ± 7,0	157 ± 47	180 ± 54
20,98 ± 0,30	21,2 ± 6,1	152 ± 44	173 ± 50
20,73 ± 0,31	18,9 ± 6,6	221 ± 77	240 ± 84
20,48 ± 0,32	24,6 ± 9,1	241 ± 89	266 ± 98
20,23 ± 0,33	29,8 ± 9,2	200 ± 62	230 ± 71
20,14 ± 0,38	40,9 ± 7,4	220 ± 40	261 ± 47
19,98 ± 0,34	35,2 ± 8,4	244 ± 59	279 ± 67
19,90 ± 0,39	25,0 ± 10,8	206 ± 89	231 ± 99
19,72 ± 0,36	30,7 ± 9,5	231 ± 72	262 ± 81
19,46 ± 0,37	22,0 ± 5,7	218 ± 57	240 ± 62
19,20 ± 0,38	19,6 ± 4,9	166 ± 42	186 ± 47
19,12 ± 0,41	18,2 ± 3,6	176 ± 35	194 ± 39
18,92 ± 0,43	19,2 ± 4,0	187 ± 39	206 ± 43
18,65 ± 0,41	14,5 ± 3,6	209 ± 52	224 ± 56

Table 5.1

Alpha production cross sections as measured by this experiment.

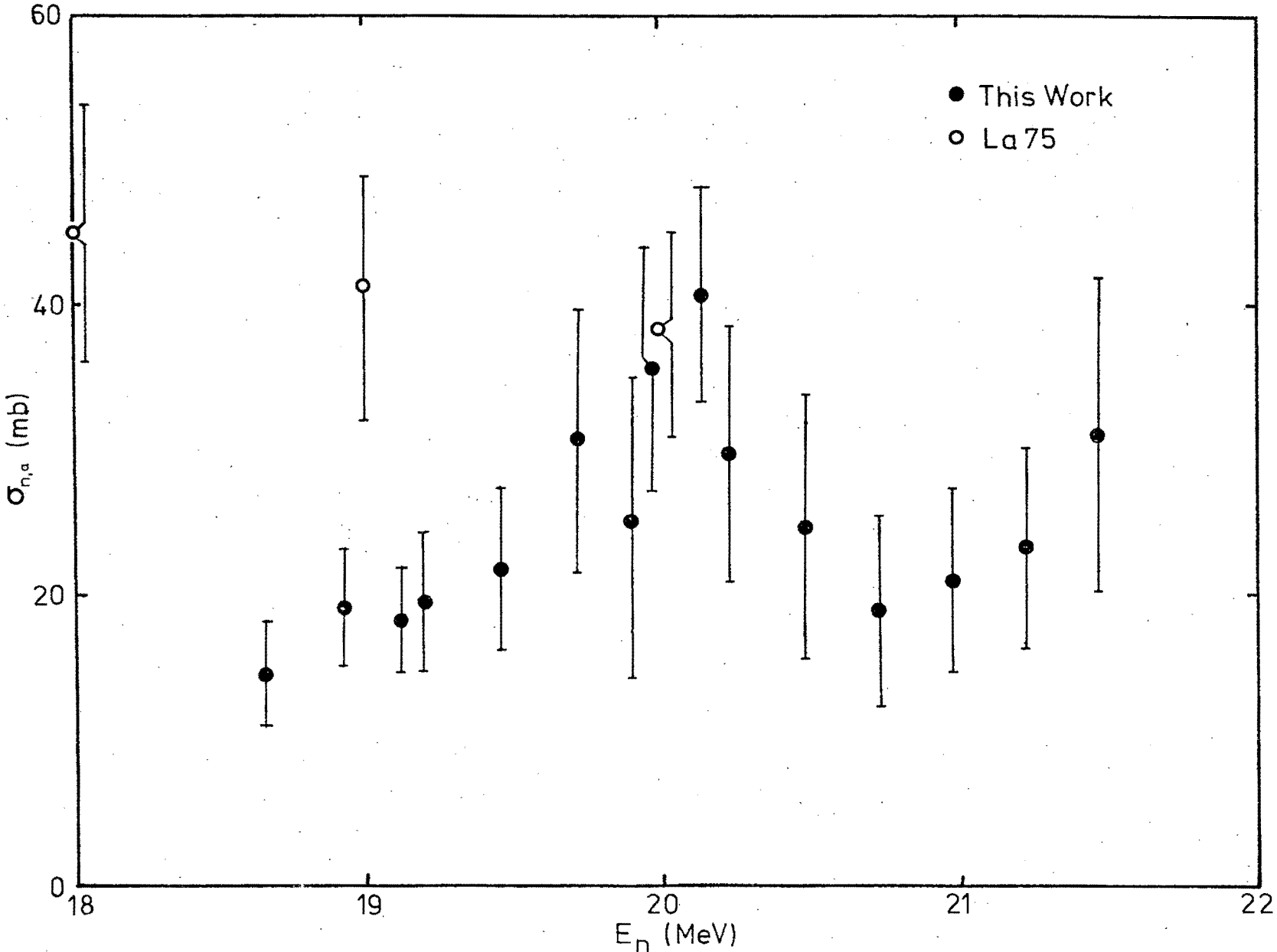

Figure 5.1

Cross sections for the $^{12}C(n,a)^{9}Be$ reaction obtained in this work, compared to the evaluated results of Lachkar et al (La75).

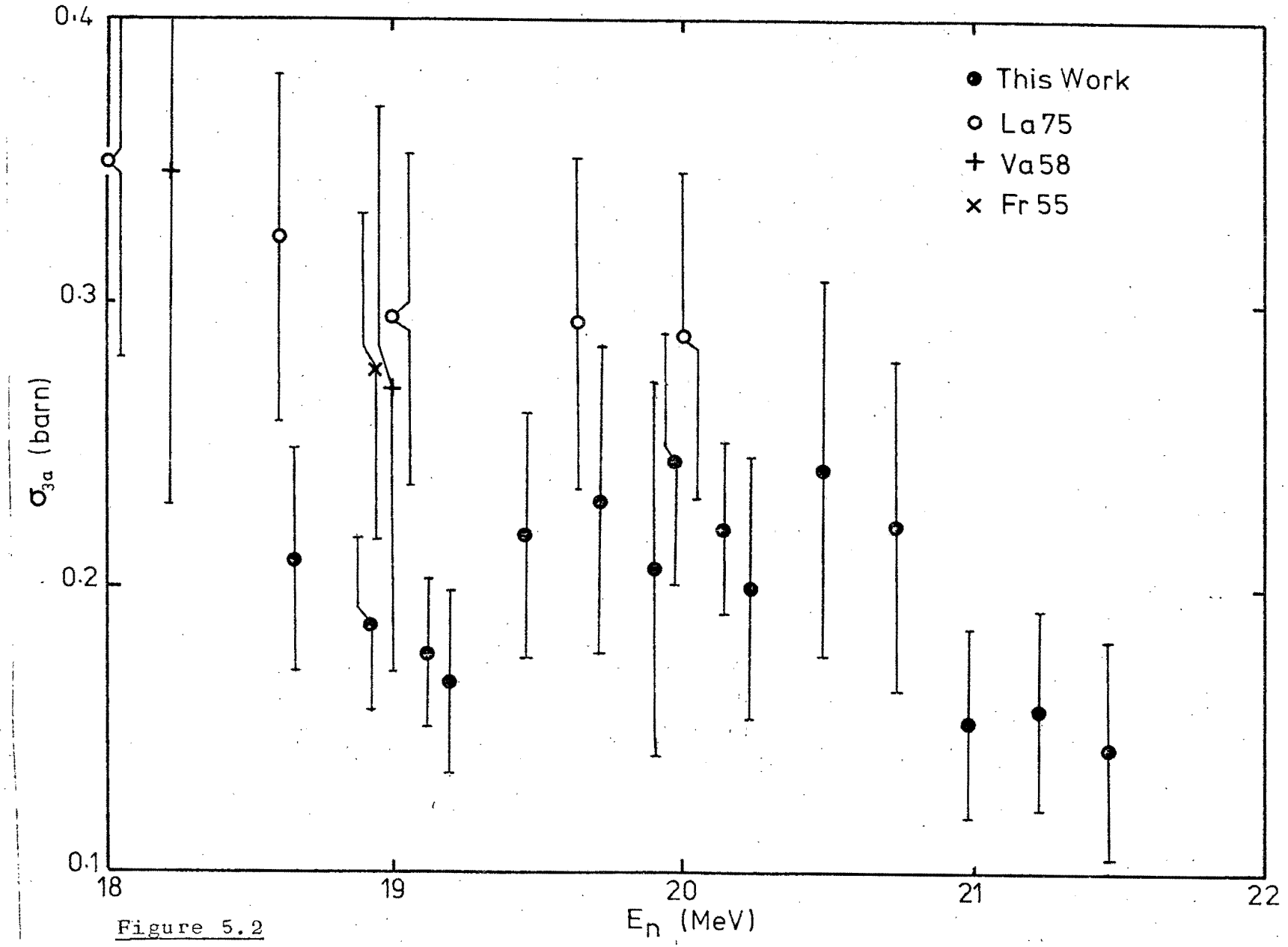

Figure 5.2

Cross sections for the $^{12}C(n,n')3\alpha$ reaction obtained in this work, compared to the values of Frye et al (Fr55), Vasil'ev et al (Va58) and Lachkar et al (La75).

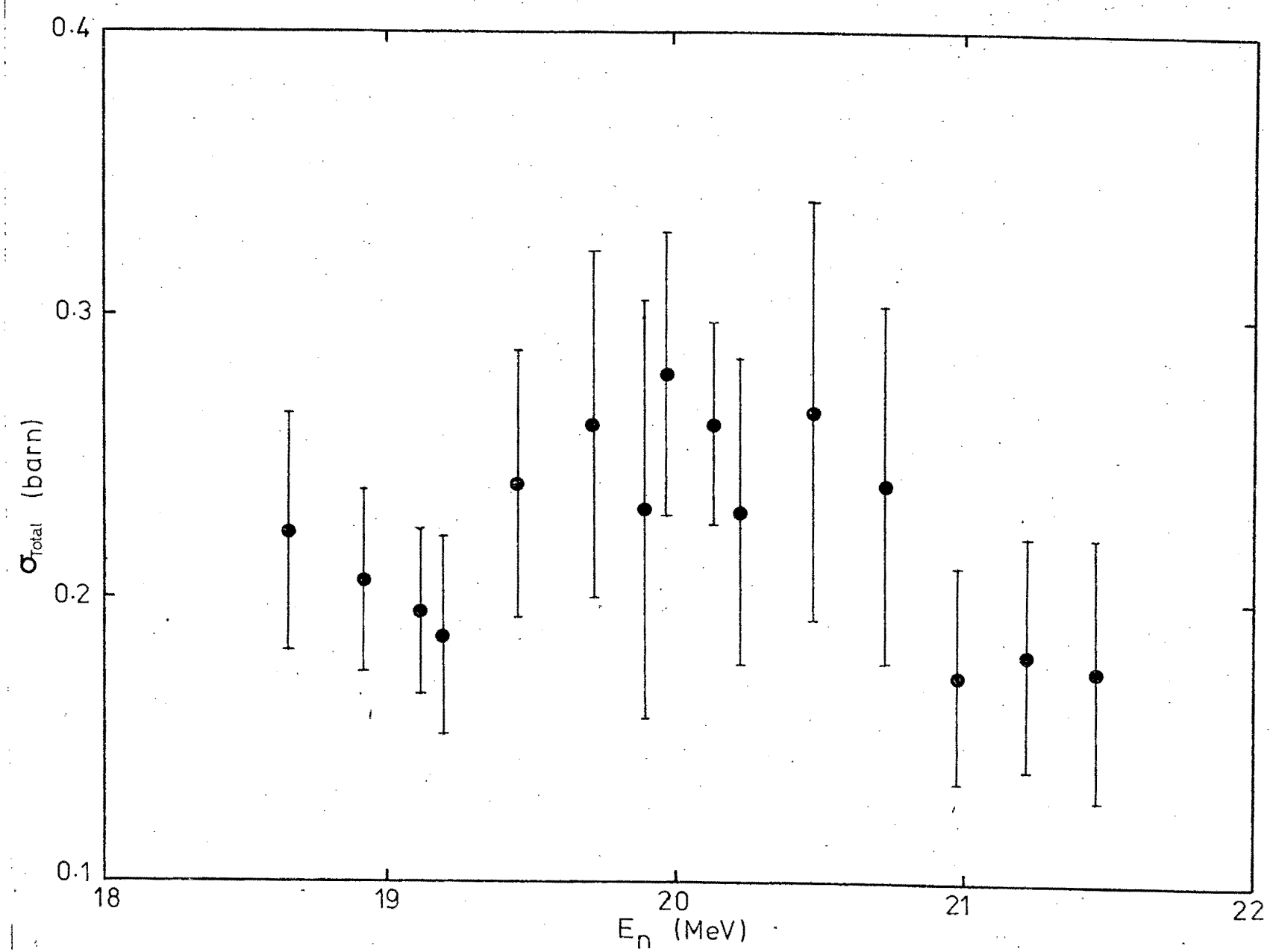

Figure 5.3

Total alpha production cross sections obtained in this work.

and 5.3, and are also presented in Table 5.1.

The errors are due mainly to the uncertainty in fitting the analytic spectra to the experimental data. Errors due to fitting were obtained by expressing the residual integral, after subtracting both analytic spectra from the experimental data, as a fraction of the experimental spectra. These errors were in the range of 20% to 30%. A further error, of approximately 5%, can be attributed to the uncertainties in the stripping process, the deuteron 'bump' integral and $\sigma_{D'}$.

5.2 Discussion

The results are self-consistent, as can be seen by referring to Table 5.1, which shows that values at overlapping energies do not show any marked deviation from each other. These results also correspond well to the data of Lachkar et al (La75) near 20 MeV. Below 20 MeV, however, the results for both the $^{12}C(n,\alpha)^{9}Be$ and the $^{12}C(n,n')3\alpha$ reactions are systematically lower than those of other authors.

An explanation could be found in the cut-off introduced in the alpha spectrum by loss of resolution caused by the alpha and proton/deuteron loci of the LS spectrum merging, as illustrated in Figure 4.2. A reduction in the bombarding neutron energy causes the alpha spectrum to 'creep' back along its locus, resulting in the loss of more and more information below the cut-off. This in turn leads to more uncertainty in the fitting of analytic spectra to the data, and could have produced the systematic effect seen. The cut-off would mainly affect the $^{12}C(n,n')3\alpha$ results as the analytic spectrum for this reaction was fitted to the experimental data near the cut-off.

43/The

The trend seen in the $^{12}C(n,\alpha)^{9}Be$ cross sections could in part be due to the cut-off, but it seems unlikely that it would affect the results as markedly as the effect observed. This is because the analytic spectrum for the $^{12}C(n,\alpha)^{9}Be$ reaction is fitted to the upper end of the experimental spectrum, which is above the cut-off for the energies considered. A comparison was also made to the results of Deconninck et al (De63) and Salathe et al (Sa71), but their values were found to be much lower by a factor of at least two. Lachkar et al (La75) mention that they rejected these results for their compilation, as they did not agree with other authors in the fairly well-known 15 - 17 MeV region, also being too low by a factor of two. It is possible, however, that the deviation from the data of Lachkar et al (La75) is valid, as their values are only evaluations.

The experiment achieved its first objective, by providing consistent measurements of the total alpha production cross section. The development of Monte Carlo models for the $^{12}C(n,\alpha)^{9}Be$ and the $^{12}C(n,n')3\alpha$ reactions made it possible to separate their contributions from the total and, therefore, to determine cross sections for them individually. No strong energy dependence of width greater than 400 KeV (defined by ΔE_n)' was found in the excitation function for the neutron energy range considered. The provision of more reliable cross sections in this poorly studied energy range should, however, be valuable.

5.3 Future Work

Future work should aim at reducing the errors inherent in these measurements. These were due largely to the uncertainty in fitting the analytic spectra to the experimental spectra. The situation could be improved by reducing the effect of the cut-off on the alpha

44/spectrum

spectrum by ensuring better resolution in that region of the LS spectrum where the alpha and proton/deuteron loci merge. The extensive use of high magnification LS spectra from the facility provided by the new data acquisition programme would improve the resolution in this important area. Much more data would, however, need to be accumulated at any one neutron energy to provide statistical significance in these expanded spectra. Because of the system used for buffering incoming data, this would require the summation of a number of runs. It is suggested that before this is attempted, some stabilisation system is installed, as difficulty was experienced during this experiment in regard to run summation, because of electronic drifts.

The development of better Monte Carlo models for the two reactions could lead to some improvements in the results, as they would match the actual conditions more closely. The $^{12}C(n,n')3\alpha$ reaction, in particular, could be represented more faithfully by using a combination of models for the various sequential processes.

A further possibility is the use of a second detector to obtain the $^{12}C(n,n')3\alpha$ spectrum independently of the $^{12}C(n,\alpha)^{9}Be$ spectrum, in a manner similar to that used by Shackleton (Sh70). This is, however, a complicated process and may not be feasible for the present type of study.

These improvements are mainly aimed at reducing or compensating for the effect of the low energy cut-off in some way. They should be considered seriously if more work is to be attempted below 18 MeV. The effect of the cut-off is automatically reduced, however, by higher energy neutrons as these will cause more of the alpha spectrum to extend past the cut-off. This could be fruitful as there is still a lack of data above 22 MeV.

REFERENCES

Al63 R.A. Al-kital and R.A. Peck Jr., Phys. Rev. 130 (1963), 1500

Aj68 F. Ajzenberg-Selove and T. Lauritsen, Nucl. Phys. A114 (1968), 1

Bi64 J.B. Birks, Theory and Practice of Scintillation Counting, Pergammon Press, 1964

Br56 F.D. Brooks, Progress in Nucl. Phys. 5 (1956), 252 (Ed. O.L. Frisch)

Br59 F.D. Brooks, Nucl. Instr. and Meths. 4 (1959), 151

Br60 F.D. Brooks, R.W. Pringle and B.L. Funt, I.R.E. Trans. Nucl. Sci. NS-7 (1960), 35

Br64 J.A. Brinkley, B.A. Robson and E.W. Titterton, Proc. Phys. Soc. 84 (1964), 201

Br74 F.D. Brooks and D.T.L. Jones, Nucl. Instr. and Meths. 121 (1974), 69

Ca55 P.O. Caldwell and J. Reginald Richardson, Phys. Rev. 98 (1955), 28

Ca71 J.A. Cahill, J. Greenwood, H. Willmes and P.J. Shaddon, Phys. Rev. C4 (1971), 1499

Ch64 M.L. Chatterjee and B. Sen, Nucl. Phys. 51 (1964), 583

Cl64 R.L. Clarke and W.G. Cross, Nucl. Phys. 53 (1964), 177

Da63 E.A. Davis, T.W. Bonner, D.W. Wosley Jr. and R. Bass, Nucl. Phys. 48 (1963), 169

De63 G. Deconninck, M. de Voey, J.P. Meulders and J. Simonet, Nucl. Phys. 49 (1963), 424

El61 M. El Nadi and H. Sherif, Nucl. Phys 28 (1961), 331

Fe53 H. Feshbach, M.M. Shapiro and V.F. Weiskopf, Tables of Penetrability for Charged Particle Reactions, NYO-3077 (1953)

Fr55 G.M. Frye, L. Rosen and L. Stewart, Phys. Rev. 99 (1955), 1375

Ga64 D.G. Gardner and Yu-wen Yu, Nucl. Phys. 60 (1964), 49

Gr49 L.L. Green and W.M. Gibson, Proc. Phys. Soc. 62 (1949), 296

Gr55 E.R. Graves and R.W. Davis, Phys. Rev. 97 (1955), 1205

Gr69 G.A. Grin, B. Vaucher, T.C. Alder and C. Joseph, Helv. Phys. Acta 42 (1969), 990

Ho68 A. Horsley, Nuclear Data A4 (1968), 321

Ja53 J.D. Jackson and D.I. Wanklyn, Phys. Rev. 90 (1953), 381

Jo62 F.A. Johnson, Canadian Journ. Phys. 41 (1962), 793

Ki69 H. Kitazawa and N. Yamamuro, Journal of Phys. Soc. of Japan 26 (1969), 600

La66 T. Lauritson and F. Ajzenberg-Selove, Nucl. Phys. 78 (1966), 1

La75 J. Lachkar, F. Cocu, G. Haouat, P. le Floch, Y. Patin and J. Sigaud, 'An Evaluation of the Neutron-Induced Scattering, Reaction and Photon-Production Cross Sections of Carbon', NEANDC (E) 168 "L" 1975

Lu70 R.L. Ludin, B.A. Wooten, R. Goloski and R.G. La Montagne, Phys. Rev. C5 (1970), 1740

Ma68 J.B. Marion and F.C. Young, 'Nuclear Reaction Analysis', North-Holland (Amsterdam), 1968

Ma75 W.R. MacMurray, Private Communication

Mo65 J. Mösner, G. Schmidt and J. Schintlmeister, Nucl. Phys. 64 (1965), 169

Mo66 J. Mösner, G. Schmidt and J. Schintlmeister, Nucl. Phys. 75 (1966), 113

Ob72 A.W. Obst, T.B. Grandy and J.L. Weil, Phys. Rev. C5 (1972), 738

Pa73 G. Pauletta, Thesis, University of Cape Town (unpublished), 1973
(Published as Pa75 q.v.)

Pa75 G. Pauletta and F.D. Brooks, Nucl. Phys. A255 (1975), 267

Pe51 J.L. Perkin, Phys. Rev. 81 (1951), 892

Re60 T. Retz-Schmidt, T.W. Bonner, G.V. Din and J.L. Weil, Bull. Am. Phys. Soc. 5 (1960), 110

Sa56 M Sachs, Phys. Rev. 103 (1956), 671

Sa71 W. Salathe, E. Baumgartner and P. Huber, Helv. Phys. Acta 44 (1971), 815

Se72 J.D. Seagrave, J.C. Hopkins, D.R. Dixon, P.W. Keaton, E.C. Kerr, A. Hiller, R.A. Sherman and R.K. Walter, Ann. Phys. 74 (1972), 250

Sh70 D. Shackleton, Thesis, University of Cape Town (unpublished), 1970

Va58 S.S. Vasil'ev, V.V. Komarov and A.M. Popova, J.E.T.P. 6 (1958), 1016

Ve68 V.V. Verbinski, F.G. Percy, J.K. Dickens and W.R. Burns, Phys. Rev. 170 (1968), 916

APPENDIX A

DATA ACQUISITION PROGRAMME

A.1 Introduction

The experiments performed by the experimental nuclear physics group at the University of Cape Town (Br74, Pa75, Sh70) generally employ the techniques used for this experiment, i.e. pulse shape discrimination and neutron time of flight. It was felt that the facilities available at the Southern Universities Nuclear Institute (S.U.N.I.) for multiparameter experiments of this nature would be improved by the provision of a data acquisition programme specially developed for these needs. In particular, better monitoring of incoming data and more extensive management of it during and after collection was required. It was decided that a three parameter data acquisition programme, providing for the buffering of all collected data on magnetic tape, together with monitoring facilities through a number of live and static displays, would best fit the total needs of the group.

The data handling facilities available to experimenters at S.U.N.I. are based on a 16 K, 18 bit word, PDP-15 computer, with a CPU capable of data manipulation and integer arithmetic. Experimental data input is accomplished through a Nuclear Data, N-parameter analogue to digital interface, with three analogue to digital converters (ADC's) on-line. Also included in the Nuclear Data, ND 50/50, system is a 4 K, 24 bit computer accessible memory unit with a display processor for displaying its contents. Other peripheral equipment consists of two magnetic tape drives, two DEC tape drives, a paper tape reader/punch, a display unit with light pen, and a console teleprinter.

A.2/A.2 Data

A.2 Data Collection

Experiments performed with PSD and neutron time of flight techniques yield three events characterized by three parameters. These are the pulse height, L, the pulse shape, S, and the neutron time of flight, T. T is usually employed as a select/reject parameter, with L and S being used to form a two parameter LS spectrum for events so selected (Br74, Pa73/5, Sh70). This system was extended so that any parameter can be chosen as the select/reject parameter, without altering the data inputs, while the other two are used to produce a two parameter spectrum. For clarity, however, the two parameter spectrum will be referred to as an LS spectrum and the select/reject parameter will be assumed to be T.

Experimental data is available to the computer through the three ADC's, which produce binary data of up to thirteen bits in length. The decision to provide an option for storing the incoming data on magnetic tape, led to the allowable conversion of the ADC's being limited to a maximum of twelve bits. This limitation permitted the use of a much simpler routine for packing the data for output to magnetic tape, as the three parameters could be stored in two 18 bit words. A routine was also provided for reprocessing the data stored on magnetic tape in exactly the same manner as the live-time data.

With a maximum of twelve bits allowed, each parameter falls in the range from 0 to 4095, permitting the generation of a 4096 x 4096 LS spectrum and a 4096 channel T spectrum. Core availability dictated that the LS spectrum be limited to a maximum of 4096 channels and the T spectrum to 512 channels. The select/reject facility was designed so that an experimenter can set a single "window" on the T spectrum to define the range of T for which events are to be accepted for analysis.

A.3/Any

Any configuration is allowed for the LS spectrum in its 4096 element matrix, e.g. 64 x 64, 32 x 128, 32 x 32, etc., of which the 64 x 64 configuration is the most common. Because of the limitation on the size of the LS spectrum it was necessary to provide an option for viewing any portion of the original 4096 x 4096 matrix, at any desired magnification, in the 4096 channels available. For clarity we limit our attention to a 64 x 64 configuration, which requires the selection of six bits from the L parameter and six bits from S. If the six high order bits are selected for both L and S, an LS spectrum is formed at the lowest possible magnification (an example is presented in Figures 2.6). This was chosen as the standard case, with a magnification of unity. If we now SHIFT our selection down one bit, an LS spectrum is formed with a magnification of two on each axis, and the overflow data is ignored. By shifting the six bit selection mask, 64 x 64 LS spectra of different magnification can be obtained, which, however, always contain the origin. To facilitate the viewing of any portion of the 4096 x 4096 spectrum it was, therefore, necessary to provide for an OFFSET to be subtracted from each parameter, which causes a redefinition of the origin. By choosing suitable SHIFTS and OFFSETS the experimenter can view any part of the LS spectrum at any desired magnification. (The LS spectrum presented in Figures 2.7 was formed for a SHIFT of 1 (magnification of 2^1) on S, a SHIFT of 2 (magnification 2^2) on L and an OFFSET on S to bring the convergence of the alpha and proton/deuteron 'ridges' into the spectrum.)

Data monitoring and management were improved by the provision of a facility whereby an experimenter can obtain real-time, single particle spectra. This was accomplished by allowing the LS spectrum to be divided into three arbitrary regions, for each of which a 512 channel L spectrum is generated during data collection. (The LS spectrum presented in Figure A.1 shows how the

A.5/regions

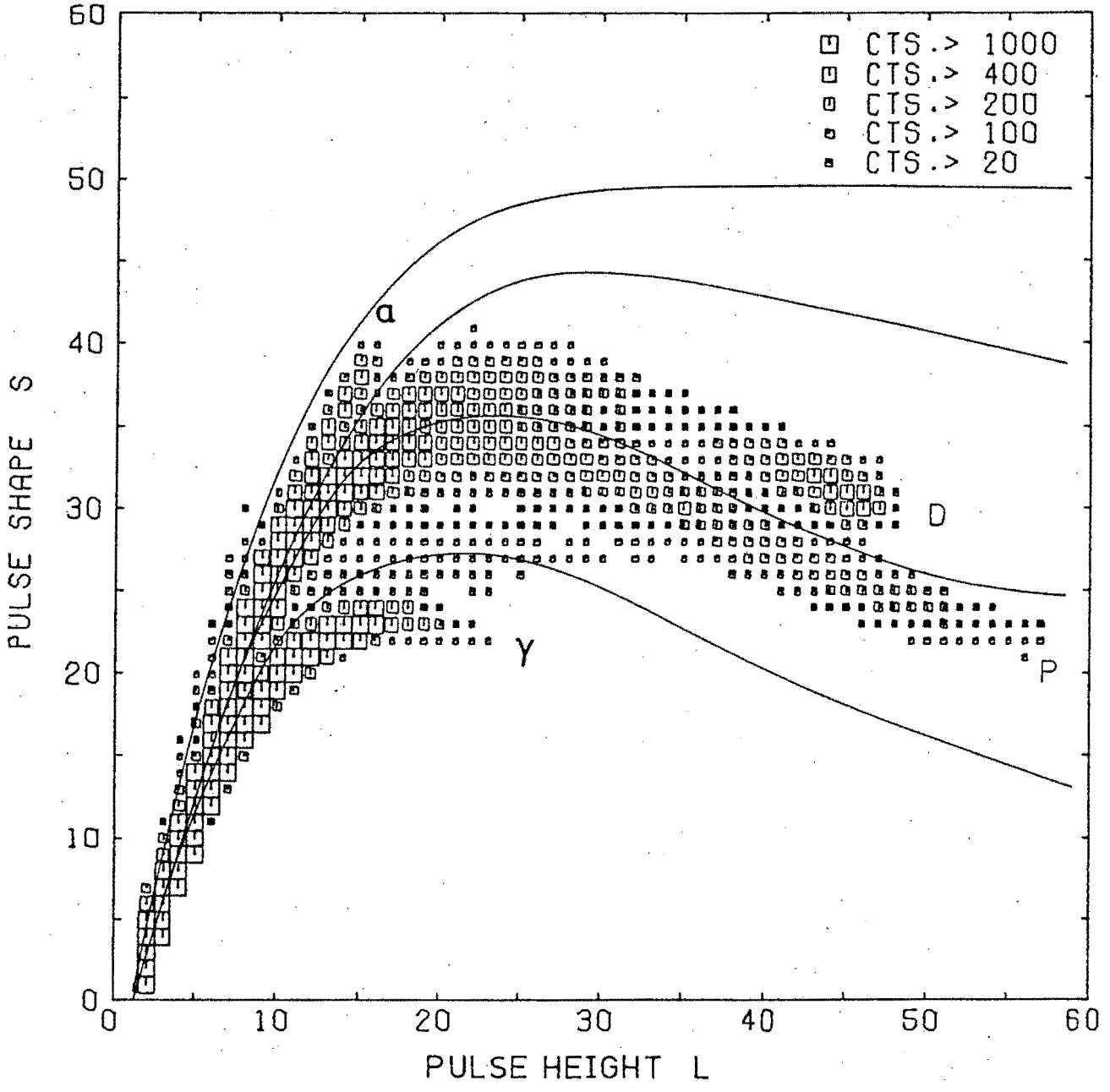

Figure A.1

Density plot of a full LS spectrum showing the boundaries that can be set to divide the spectrum into three regions.

regions were defined during this experiment to produce real-time spectra for alphas, protons and deuterons.) The experimenter can also decide before a data collection run whether events where LS co-ordinates fall outside these regions are to be accepted or rejected.

A set of internal scalers was also included to provide run time statistics to the user. These monitored the integrals of the three single particle L spectra, the integral of the T spectrum, the number of data blocks written onto magnetic tape, and the number of events accepted and rejected.

A.3 Displays and Related Routines

A number of live and static display routines, using the computer CRT, were developed to provide the experimenter with information on the contents of the various spectra and the scalers. A contour display was chosen for the LS spectra whereby it was represented by a 4096 dot matrix. The four 512-channel spectra are displayed simultaneously, one above the other, in the usual 'counts-versus-value' format. A numeric display routine was included for displaying the contents of the scalers. These three routines are available as both static and live displays. A further live display option provided is a flying spot display of the latest LS event accepted.

The light pen facility attached to the CRT is utilised by a number of interactive display routines. An option for the static contour display allows the user to set the boundaries of the regions discussed in the previous section, by using the light pen to mark their positions on the dot matrix. The "window" on the T spectrum is set in like fashion, by using the light pen to mark its upper and lower limits on the single parameter spectrum

A.6/display

display. Another routine incorporated in the data acquisition programme provides the user with the capability of integrating the single parameter spectra. The limits of integration are also set using the light pen with the spectrum display, and results are printed out on the console teleprinter.

A.4 Input/Output Routines

The size of the data acquisition programme made it impossible to use the Input/Output (I/O) device handlers provided with the operating system. It was, therefore, necessary to develop simplified handlers for the I/O devices employed. Apart from the ADC servicing and display routines, handlers were provided for the console teleprinter, the magnetic tape units and the ND 50/50 system.

At the time of development only one magnetic tape drive was under computer control, the other one being connected to the ND 50/50 system. The need for transporting the LS and single particle spectra to other computing facilities prompted the inclusion of routines for transferring these spectra to the ND 50/50 memory. This allows the user to write the data onto magnetic tape, and to make use of the ND 50/50 display processor.

To facilitate the speedy retrieval of data from the computer controlled magnetic tape, it was decided that each set of data so stored, should be terminated by a filemark. A routine was provided for positioning data for input by searching for a specified tag.

A.7/A.5 Improvements

A.5 Improvements

Since implementation of this data acquisition programme, S.U.N.I. has added a further two DECtape units, a PDP-11 controlled, disc orientated mass storage system, a video terminal, a further 16 K of core memory, and a line printer to the system. These hardware additions were accompanied by a disc-resident, time sharing operating system. The data acquisition programme is not, however, compatible with this operating system and should be altered so that the full potential of the time sharing environment can be realised. Compatibility with the operating system would allow DEC tape to be offered as an alternative to magnetic tape.

A number of additional options can possibly be offered to users by making use of the new peripheral equipment. Better CPU utilisation for data collection can be achieved by using the video terminal to display certain information, instead of the CRT display unit. The line printer can be employed to provide hardcopy of the contents of the spectra, using programmes already available at the University of Cape Town. The disc mass storage system offers possibilities for accumulating LS spectra with more than 4096 channels, and for fast buffering of incoming data during high count rate experiments.

These additions would require major changes to the programme and its methods of interaction with peripheral devices. A useful addition, requiring little alteration, however, would be the provision of a software controlled digital stabiliser. This would be a welcome improvement as electronic drifts cause a number of problems.

APPENDIX B

MONTE CARLO MODELS

The $^{12}C(n,\alpha)^{9}Be$ reaction was analysed using the formula presented in Figure B.1, viz.:

$$E_3/E_T = B + D + 2(AC)^{\frac{1}{2}}\cos\theta$$

where A, B, C and D are expanded in Figure B.1;
E_3 is the energy of the emitted alpha;
E_T is the total energy available to the reaction; and
θ is the angle of emission of the alpha in the centre of mass frame.

The corresponding formula for the energy of the ^{9}Be nucleus is:

$$E_4/E_T = A + C + 2(AC)^{\frac{1}{2}}\cos\phi$$

where E_4 is the energy of the ^{9}Be nucleus, and
$\phi = \pi - \theta$

The angular distribution of the alphas in the centre of mass frame was assumed to be isotropic, and for this reason θ was found by sampling the interval $(0, \pi)$ in a random manner. A psuedo random number generator, producing numbers randomly and uniformly distributed on the interval (0,1) was used for this purpose.

Barrier penetrability was introduced by ensuring that the energies calculated, sampled the energy distribution determined by this effect (Fe53). Sampling of this distribution was implemented by employing another random number, x, normalised to the range of probabilities. Events were only accepted for:

$$x \leqslant P(E_\alpha)$$

ψ, ζ in lab.

θ, ϕ in c.m.

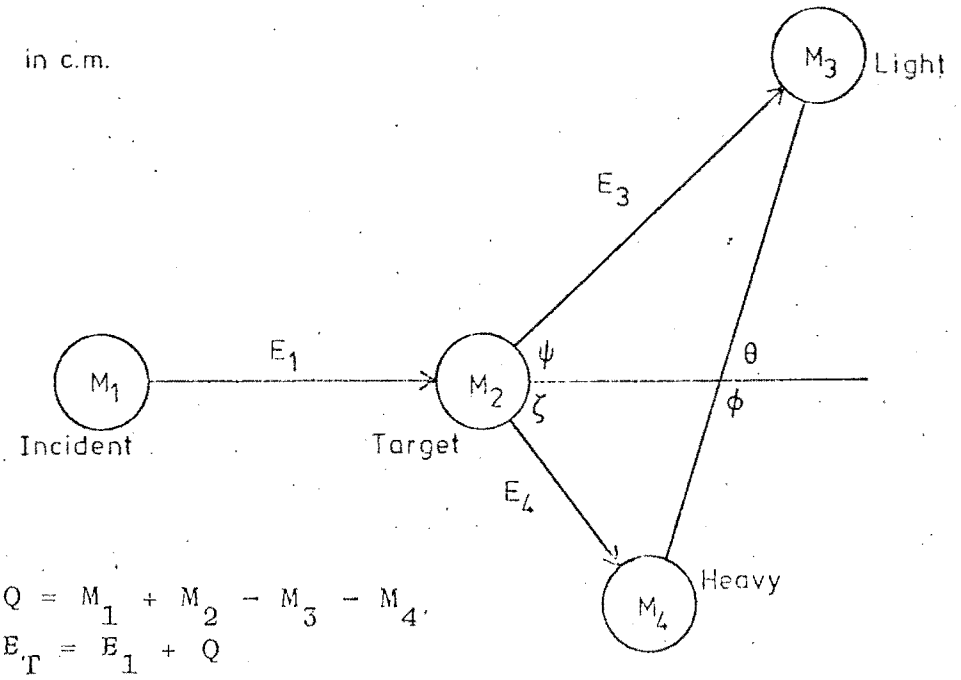

$$Q = M_1 + M_2 - M_3 - M_4$$

$$E_T = E_1 + Q$$

Define:

$$A = \frac{M_1 M_4 (E_1/E_T)}{(M_1 + M_2)(M_3 + M_4)}$$

$$B = \frac{M_1 M_3 (E_1/E_T)}{(M_1 + M_2)(M_3 + M_4)}$$

$$C = \frac{M_2 M_3}{(M_1 + M_2)(M_3 + M_4)} \left[1 + \frac{M_1 Q}{M_2 E_T} \right]$$

$$D = \frac{M_2 M_4}{(M_1 + M_2)(M_3 + M_4)} \left[1 + \frac{M_1 Q}{M_2 E_T} \right]$$

The laboratory energies of the two products are then given by the equations:

$$\frac{E_3}{E_T} = B + D + 2(AC)^{\frac{1}{2}} \cos\theta \quad \text{and} \quad \frac{E_4}{E_T} = A + C + 2(AC)^{\frac{1}{2}} \cos\phi$$

Figure B.1

Formula used for the model of the $^{12}C(n,\alpha)^{9}Be$ reaction. (Reproduced from Marion and Young (Ma68).)

$$x \leqslant P(E_\alpha)$$

where $P(E_\alpha)$ is the energy distribution determined by the barrier penetrability.

The crystal response to the alpha was determined by using a table of values for Brooks' response curves for anthracene (Br56). The response to the ^{9}Be nucleus was determined by assigning to it a 2+ charge state. This permitted the table of values for the alpha response to be used because it leads to the relation:

$$L_{Be}(E) = \frac{9}{4} L_\alpha(\frac{4}{9} E)$$

The sum of these responses was then used for forming the pulse height spectrum.

The model of the $^{12}C(n,n')3\alpha$ reaction was developed using a four particle phase space distribution for the energies of the emitted neutron and alphas (Fr55). This distribution is:

$$N(\varepsilon)d\varepsilon = \text{const}\sqrt{\varepsilon}\,(1 - \varepsilon)^2 d\varepsilon$$

where ε is the ratio of the energy of the particle to the maximum energy it can have. This distribution was sampled for each of the three alphas, using pairs of random numbers as described above. Events were only accepted if the sum of the alpha energies was less than the total available to the reaction, i.e. conservation of energy. The excess energy was assumed to be removed by the neutron. Responses were determined as for the $^{12}C(n,\alpha)^{9}Be$ model, and their sum was used for forming the pulse height distribution. Flowcharts of these two models are presented on the following pages.

$^{12}C(n,\alpha)^{9}Be$ Monte Carlo Model